RESEARCH ARTICLE

ISEV

Reversing the surface charge of MSC-derived small extracellular vesicles by εPL-PEG-DSPE for enhanced osteoarthritis treatment

Kai Feng[1] | **Xuetao Xie**[1] | **Ji Yuan**[1] | **Liangzhi Gong**[1] | **Zhaochen Zhu**[1] |
Juntao Zhang[1] | **Haiyan Li**[2] | **Yunlong Yang**[1] | **Yang Wang**[1]

[1] Institute of Microsurgery on Extremities, Department of Orthopedic Surgery, Shanghai Jiao Tong University Affiliated Sixth People's Hospital, Shanghai, China

[2] Chemical and Environmental Engineering, School of Engineering, RMIT University, Melbourne, Australia

Correspondence
Yunlong Yang and Yang Wang, Institute of Microsurgery on Extremities, Department of Orthopedic Surgery, Shanghai Jiao Tong University Affiliated Sixth People's Hospital, No. 600 Yishan Road, Shanghai 200233, China.
Email: yunlong0424@outlook.com and wangyang63@sjtu.edu.cn

Abstract

Mesenchymal stem cell-derived small extracellular vesicles (MSC-sEVs) possess a great therapeutical potential for osteoarthritis (OA) treatment. However, the steric and electrostatic hindrance of cartilage matrix leads to very limited distribution of MSC-sEVs in cartilage and low bioavailability of MSC-sEVs after intra-articular injection. To overcome this, a strategy to reverse the surface charge of MSC-sEVs by modifying the MSC-sEVs with a novel cationic amphiphilic macromolecule namely ε-polylysine-polyethylene-distearyl phosphatidylethanolamine (PPD) was developed in this study. Through incubation with 100 μg/ml PPD, positively charged MSC-sEVs (PPD-sEVs) were obtained, and the modification process showed nearly no disturbance to the integrity and contents of sEVs and exhibited good stability under the interference of anionic macromolecules. A more effective cellular uptake and homeostasis modulation ability of PPD-sEVs than unmodified MSC-sEVs to chondrocytes was demonstrated. More importantly, PPD-sEVs demonstrated significantly enhanced cartilage uptake, cartilage penetration, and joint retention capacity as compared to MSC-sEVs. Intra-articular injection of PPD-sEVs into a mouse OA model showed significantly improved bioavailability than MSC-sEVs, which resulted in enhanced therapeutic efficacy with reduced injection frequency. In general, this study provides a facile and effective strategy to improve the intra-articular bioavailability of MSC-sEVs and has a great potential to accelerate the clinical practice of MSC-sEVs based OA therapy.

KEYWORDS
MSC derived small extracellular vesicles, osteoarthritis, surface charge reverse, surface modification

1 | INTRODUCTION

Osteoarthritis (OA) is a highly prevalent joint disease that affects over 240 million people worldwide, posing a severe threat to the public health (Katz et al., 2021). However, so far, no disease modifying drug has been successfully applied due to the complexity of OA pathology (Hunter & Bierma-Zeinstra, 2019). Mesenchymal stem cell derived small extracellular vesicles (MSC-sEVs) have attracted much attention in OA therapy. These nanosized (30–150 nm) vesicles can transfer a variety of bioactive molecules to damaged cartilage and exert positive modulation. MSC-sEVs can modulate cartilage homeostasis by inhibiting inflammation, promoting chondrocyte proliferation, and enhancing matrix deposition (Ruiz et al., 2020; Woo et al., 2020; Wu et al., 2019). Furthermore, they can also alleviate cell senescence (Tofiño-Vian et al., 2017). Therefore, MSC-sEVs are capable to modulate

many aspects of OA related pathology, such as metabolic disorder and ageing, laying their solid foundation as cell free therapeutic factors for OA therapy.

Intra-articular injection provides an appropriate administration method for MSC-sEVs deployment, and the effective distribution of MSC-sEVs in cartilage after intra-articular injection is critical for their loadings delivery (Wehling et al., 2017). Cartilage matrix is mainly woven by type II collagen networks filled with dense and anionic aggrecan proteoglycans and presents very small pores (<6 nm) for solute penetration (Kiani et al., 2002; Mow et al., 1984). A recent study uncovers that sEVs can traverse extracellular matrix (ECM) networks with mesh size smaller than their own by aquaporin-mediated deformability (Lenzini et al., 2020). However, the highly negatively charged cartilage matrix also presents an electrostatic hinderance for these sEVs whose surface is constructed by anionic phospholipid (Bajpayee & Grodzinsky, 2017; Bajpayee et al., 2014). The electrostatic repulsion can induce a strong distribution tendency of sEVs in synovial fluid rather than in cartilage according to Donnan's theory (Stell & Joslin, 1986). However, sEVs in synovial fluid are also cleared fast due to the elimination effect of capillary and lymph-vessel in synovia membrane on nanoparticles (Pradal et al., 2016). All these factors result in a low intra-articular bioavailability of MSC-sEVs, and frequent injections of high dose MSC-sEVs are essential in related studies (Zhang et al., 2016, 2018; Zhu et al., 2017). Therefore, enhancing the bioavailability of intra-articularly injected MSC-sEVs is the top priority for their future clinical application.

Cationic nanocarriers have been widely studied in intra-articular drug delivery (Colella et al., 2020; Vedadghavami et al., 2020). These nanocarriers can be adsorbed fast by cartilage in the aid of the electrostatic interaction with anionic cartilage matrix components, which prevents their intra-articular clearance and further leads to their deep penetration and long-time residence. Inspired by the strategy, we envision that reversing the negative surface charge of MSC-sEVs would enhance their intra-articular bioavailability for OA therapy. Recently, a few studies have successfully grafted cationic molecules to sEVs by cationic polymer adsorption (e.g., polyethyleneimine [PEI]), covalent modification, or cationic liposome fusion (Hwang et al., 2019; J. Kim, Lee, et al., 2020a; Piffoux et al., 2018; Tamura et al., 2017; Zhupanyn et al., 2020). However, all these methods show disruption to sEVs and face some problems for application. For instance, the applied cationic polymers are usually toxic, able to break the lipid membrane and induce the cluster of sEVs (Fischer et al., 1999; Zhupanyn et al., 2020). In addition, the widely distributed anionic biomacromolecules in joint can interfere in the electrostatic interaction, such as hyaluronic acid (HA) and chondroitin sulfate (CS), leading to an unstable modification (Danielsen et al., 2005; Ma et al., 2017; Wang et al., 2012). Covalent modification often involves in toxic agents and can disturb the surface proteins (Yang et al., 2021). While, liposome fusion increases the size of sEVs, which may further compromise their cartilage penetration (Sato et al., 2016). Therefore, a suitable modification method should be established not only to reverse the surface charge but also maintain the therapeutical functions and properties of MSC-sEVs as much as possible.

In this study, in order to enhance the intra-articular bioavailability of MSC-sEVs for OA therapy, positively charged MSC-sEVs are developed by simply incubating them with a novel cationic amphiphilic macromolecule ε-polylysine (εPL) -polyethylene (PEG) - distearyl phosphatidylethanolamine (DSPE; PPD) (Figure 1A). In PPD, εPL is chosen as the cationic moiety to adsorb to sEVs surface and synchronously reverse the surface charge. εPL is a cationic poly amino acid (25 ~ 35 lysine monomers) secreted by *Streptomyces* and shows excellent biocompatibility (Bankar & Singhal, 2013; Shima & Sakai, 1977). The US Food and Drug Administration (FDA) approved PEG-DSPE is conjugated to εPL to further stabilize the charge reverse under the interference of anionic macromolecules in joint space by inserting into the lipid membrane of sEVs. In addition, sEVs secreted by induced pluripotent stem cell derived MSC (iMSC-sEVs) were used in this study due to their better performance than sEVs secreted by adult tissues derived MSCs in OA modulation, functional stability, and batch production ability (G. W. Hu et al., 2015; Jiang et al., 2019; Zhu et al., 2017). Our findings show that the surface charge of the iMSC-sEVs can be efficiently reversed from electronegativity to electropositivity by PPD modification, which increases their uptake, penetration, and retention in cartilage, leading to an enhanced OA treatment. This study provides not only a novel strategy for an effective MSC-sEVs based OA therapy but also a simple and effective method for reversing the surface charge of sEVs, which would extend and benefit the applications of MSC-sEVs for treatments of many other diseases.

2 | MATERIALS AND METHODS

2.1 | Materials

εPL (Mw 4.6 KDa, tested by GPC) was purchased from Bainafo Bioengineering Co. Ltd (Zhengzhou, China). Succinate ester of DSPE-PEG (DSPE-PEG-NHS, Mp: 2 KDa) was synthesized by SinoPEG Bioengineering Co. Ltd (Xiamen, China). Rhodamine B isothiocyanate, bovine serum albumin (BSA), and dimethyl sulfoxide (DMSO, AR) were obtained from Sigma Aldrich (MO, USA). Lipid membrane fluorescent dyes DiO, DiI, and DiR were purchased from Thermo Fisher Scientific (MA, USA). Fetal bovine serum (FBS), collagenase II, 100 U/ml penicillin G and 0.1 mg/ml streptomycin were purchased from Gibco (CA, USA). PBS and Dulbecco's modified Eagle's medium (DMEM)-F12 were obtained from HyClone (UT, USA). 4′,6-diamidino-2-phenylindole (DAPI), Annexin-V-FITC Apoptosis Detection kit, BeyoClick 5-ethylnyl-2′-deoxyuridine (EdU) Cell Proliferation
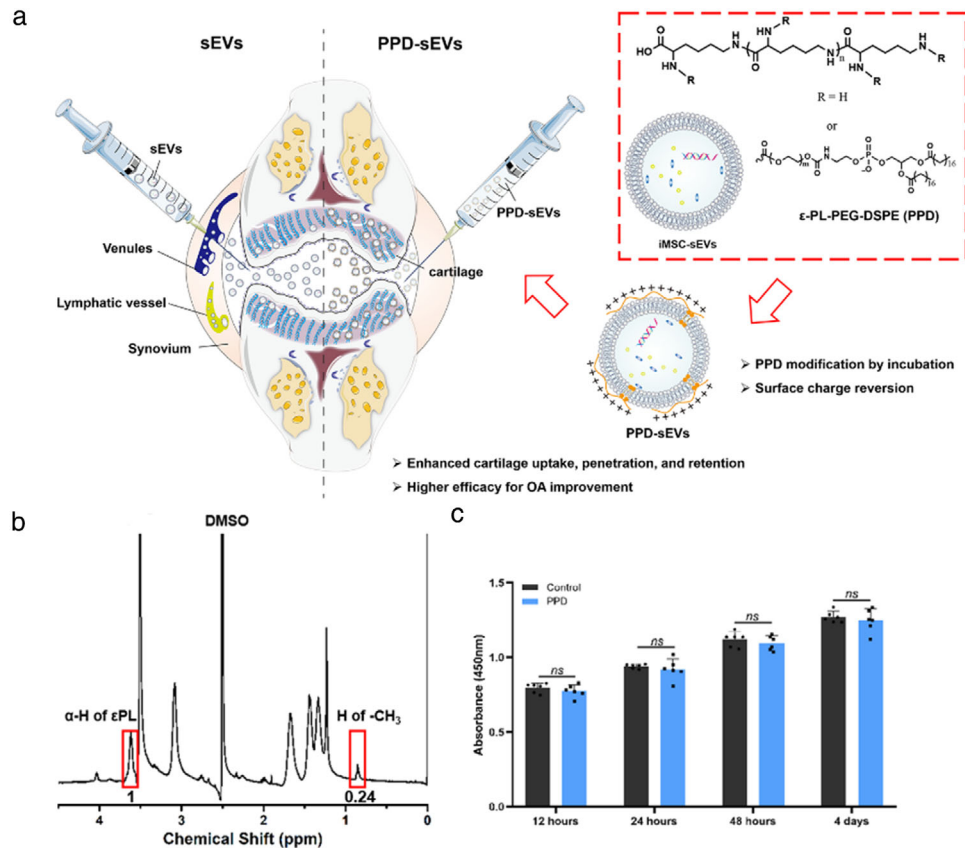
FIGURE 1 Schematic illustration of surface charge reverse strategy and PPD characterization. (A) Schematic illustration of the surface charge reverse strategy of sEVs by PPD modification for their enhanced cartilage biodistribution; (B) ^{1}H-NMR (400 M) spectrum of PPD (DMSO-d_6); (C) The cytocompatibility of 100 μg/ml PPD detected by CCK8 assay ($n = 6$)

kit with Alexa Fluor 488, and One Step TdT-mediated dUTP Nick-End Labeling (TUNEL) Apoptosis Assay kits were purchased from Beyotime Biotechnology (Jiangsu, China). Interleukin-1β (IL-1β) was obtained from R&D system (MN, USA). The information of the antibodies used in this study was listed in Table S1.

2.2 | Synthesis and characterization of PPD

PPD was synthesized by the amide ligation between εPL and DSPE-PEG-NHS. Briefly, 200 mg εPL were dissolved in 5 ml double distilled water (DDW), and the solution pH was adjusted to 8 ~ 9 by 1 M NaOH. Then, 3 ml DMSO was added to the above solution. After that, 100 mg DSPE-PEG-NHS were dissolved in 2 ml DMSO, and the solution was added dropwise to εPL solution, followed by stirring for 24 h at room temperature. Finally, the reaction solution was diluted by DDW and dialyzed against water/DMSO. After lyophilization, PPD (150 mg) was obtained as white floc. ^{1}H nuclear magnetic resonance (^{1}H-NMR) and Matrix-assisted laser desorption/ionization time of flight mass spectrometry (Moldi-Tof MS) were used to characterize PPD.

2.3 | Preparation and characterization of PPD modified iMSC-sEVs

Small extracellular vesicles secreted from induced pluripotent stem cell (iPSC) derived MSC (iMSC) were used in this study. The derivation of iMSC was generated from an iPSC cell line (iPS-S-01) provided by the Institute of Biochemistry and Cell Biology of the Chinese Academy of Sciences according to our previous reports (Liu et al., 2017). iMSC were cultured in the serum-free ncMission hMSC Medium (RP02010, Nuwacell Biotechnologies Co., Ltd, China) and the medium was replaced every two days. After reaching 80%–85% confluency, iMSC-sEVs (sEVs) were isolated and purified by differential ultracentrifugation. Briefly, the culture medium was centrifuged at 300g for 20 min and 2000g for 30 min. After that, large EVs were removed by high-speed centrifugation (10,000g) for 60 min and filtration through a 0.22 μm filter (Millipore, MA, USA). Next, the supernatant was further ultracentrifuged at 100,000g for 114 min (ultracentrifuge Optima XPN with a SW32 Ti rotor, Beckmann Coulter, USA).

After removing the supernatant, sEVs pellets were resuspended in PBS, followed by another ultracentrifugation at 100,000*g* for 114 min. All procedures were performed under 4°C. Ultimately, the pelleted sEVs were resuspended in PBS and preserved at −80°C at most 1 month before use.

To achieve the charge reverse, isolated sEVs (1×10^{10} particles/ml) were incubated with the PBS solution containing various concentration of PPD or RITC labelled PPD for 60 min at room temperature. After incubation, 1 ml mixed solution were diluted with 100 ml sterile PBS to eliminate PPD aggregation. Then, the diluted solutions were purified by ultracentrifugation to obtain PPD-sEVs. Meanwhile, to further confirm whether PPD could be isolated with PPD-sEVs by ultracentrifugation, 1 ml single RITC-PPD in PBS solution at the concentration of 100 μg/ml was diluted in 100 ml PBS solution and then purified by ultracentrifugation. Subsequently, the bottom of the ultracentrifuge tube was resuspended with PBS and detected by a multifunctional microplate reader named Varioskan LUX (Thermo Fisher Scientific, USA).

To validate whether PPD modification could alter the integrity and contents of sEVs, a series of experiments were performed.

2.3.1 | Nano-flow cytometry

First, a nano-flow cytometry (N30 NanoFCM, Xiamen, China) was used to detect the modification of PPD (or RITC-PPD) to sEVs surface. Modified or unmodified sEVs suspensions were added to the nano-flow cytometry, then PPD modification rate and the size distribution were evaluated by this machine.

2.3.2 | Surface charge analysis

Surface charge of unmodified sEVs and PPD modified sEVs was detected by a nanoparticle analyzer (DelsaMax Pro, Beckman Coulter, USA).

2.3.3 | Transmission electron microscopy (TEM)

According to the published protocols (Xia et al., 2021), TEM and cryo-TEM analysis were used for morphology observation of sEVs. For TEM observation, unmodified sEVs or PPD-sEVs suspensions were dropped onto a formvar-carbon-coated grid and dried in air for 20 min. Then, the grids were rinsed with sterile PBS and fixed in 1% (w/v) glutaraldehyde for 5 min. The grids were further rinsed with deionized (DI) water and stained with 2% (w/v) uranyl oxalate for 5 min. After drying, the microstructure of unmodified sEVs or PPD-sEVs were observed by TEM (Hitachi H-7650, Tokyo, Japan). For cryo-TEM observation of unmodified sEVs and PPD-sEVs, the sEVs were added onto the lacey carbon grid (Electron Microscopy Science, PA, USA). The grid was frozen in liquid nitrogen and then the surface structure of each sample was analyzed by using a Tecnai F20 Twin transmission electron microscope.

2.3.4 | Protein concentration assay

Protein concentration of unmodified sEVs and PPD-sEVs were quantified by Pierce BCA Protein Assay Kit (Cat#23225, Thermo Fisher Scientific, USA). Briefly, unmodified sEVs and PPD-sEVs at the concentration of 1×10^{10} particles/ml were digested with RIPA lysis buffer (Beyotime, Jiangsu, China), and the proteins were harvested following the manufacturer's instructions. Next, a total of 10 μl protein sample or single PPD solution was loaded into each well of a 96-well-plate and 200 μl of the working reagent was added. Subsequently, the plate was incubated for 30 min at 37°C and the absorbance was measured at 562 nm by a multifunctional microplate reader (Varioskan LUX, Thermo Fisher Scientific, USA). The standard curve was used to determine the protein concentration of sEVs sample in each group.

2.3.5 | Western blot

To detect the expressions of classical surface markers in unmodified sEVs and PPD-sEVs, the protein samples were collected from unmodified sEVs, PPD-sEVs and iMSC using RIPA lysis buffer (Beyotime, Jiangsu, China). The Western Blot analysis were performed as described previously (Gong et al., 2020). Briefly, after being incubated with 5% BSA for 60 min at room temperature for blocking the unspecific absorption, the polyvinylidene difluoride (PVDF) membranes were incubated with primary antibodies including TSG101 (1:1000), CD63 (1:1000), CD9 (1:1000), GM130 (1:1000), Lamin A/C (1:1000), and β-actin (1:1000) overnight at 4°C. Subsequently, the PVDF membranes were incubated with horseradish peroxidase (HRP)-labeled secondary

antibody at room temperature for 60 min and chemiluminescent signals were visualized by the ECL Western Blot detection kit and Bio-RAD imaging system (Bio-RAD, CA, USA). In addition, to further investigate whether PPD modification could impact the content of the inner proteins in sEVs, six selected chondro-protective proteins (AGRN, TGFB2, TGFBI, TIMP1, TIMP2, and TIMP3) that show potential chondro-protective functions according to previously published articles were detected by Western Blot analysis (Eldridge et al., 2016; Jhun et al., 2021; Li et al., 2019; Mi et al., 2012; Ruiz et al., 2020). Moreover, CD73 and its downstream pathway related proteins, including total Akt, p-Akt, total Erk, and p-Erk, were also analyzed by Western Blot to confirm whether PPD would shield the function of sEVs' surface proteins.

2.3.6 | RNA concentration assay

To detect and compare the total RNA amounts in unmodified sEVs and PPD-sEVs, SYTO® RNASelect™ Green Fluorescent Cell Stain Kit (S32703, Life technology, UK) was used to labelling of RNA in sEVs and PPD-sEVs in vitro. Briefly, 1 μl of the dye stock solution was added to the 100 μl unmodified sEVs (1×10^{10} particles/ml) and PPD-sEVs (1×10^{10} particles/ml) sample, and the mixed solution was incubated at 37°C for 20 min. Then we removed excess unincorporated dye from the labelled sEVs and detected the efficiency of labelling RNA (488 nm excitation) in each group using the Varioskan LUX. Total RNA amount in each group was calculated, and then the relative expression of total RNA in each group was normalized against the unmodified sEVs group.

2.3.7 | Quantitative real-time PCR analysis

To explore whether PPD modification could affect the specific RNA content of sEVs, six selected chondro-protective microRNAs (miR-100-5p, miR-23a-3p, miR-3960, miR-92a-3p, miR-155-5p, and miR-221-3p) (H. Hu et al., 2020; Mao et al., 2018; Woo et al., 2020; Wu et al., 2019) in sEVs and PPD-sEVs were detected. PCR analysis was performed as described previously (Chen et al., 2019). Total microRNAs in the sEVs group and the PPD-sEVs group were isolated by using the Exosome RNA Purification Kit (Qiagen, Germany), and the reverse transcription reactions of microRNAs were performed using the 4 × Reverse Transcription Master Mix kit (EZBioscience, USA). Subsequently, the qRT-PCR analysis of microRNAs was carried out with FastStart Universal SYBR Green Master (Roche, Germany). The stem-loop RT primers and the gene-specific primers are listed in Table S2.

2.4 | The stability of PPD-sEVs

To evaluate the stability of PPD modification on sEVs, the PPD modification rate and average particle diameter of PPD-sEVs were detected by the nano-flow cytometry, and surface charge was detected by the nanoparticle analyzer. PPD-sEVs or RITC labeled PPD-sEVs were placed for a 7-day period at room temperature. The above parameters were monitored at preset time point (0, 1, 3, and 7 day).

Moreover, to further explore the stability of PPD-sEVs in joint cavity, 1×10^{10} particles/ml RITC labelled PPD or RITC labelled εPL modified sEVs were incubated with gradient concentrations of HA (Mw 100 KDa) and CS (Mw 50 KDa) solution (5, 10, 20 mg/ml) for 24 h at 37°C. After the sEVs were incubated in different concentration of HA and CS solution, the solution was filtered by a 0.22 μm membrane. Then, the sEVs were isolated by standard ultracentrifugation and the PPD or εPL modification rate in each group was analyzed by the nano-flow cytometry. To further investigate the time-dependent stability under physiologically mimicking environment, surface modified sEVs were incubated with 10 mg/ml HA or CS at 37 °C for 1, 2, 3, and 7 day. After incubation, the sEVs were isolated by 0.22 μm filtration and standard ultracentrifugation, then the modification rate was detected by the nano-flow cytometry.

2.5 | Human chondrocytes isolation and culture

All procedures in this research were approved by the Independent Ethics Committee of Shanghai Jiao Tong University Affiliated Sixth People's Hospital (Approval Number: 2020-YS-154, March 30, 2020, Shanghai, China). Written informed consent was provided from the patient and patient's parents. Human chondrocytes were isolated from normal knee joint cartilage of a young patient (male, aged 14) with distal osteoma in lower limb and no history of OA. As previously reported, the harvested cartilage was cut into 1 mm^3 and incubated with 0.25% collagenase II in DMEM-F12 medium supplemented with 1% Penicillin-Streptomycin at 37°C for 4 h. Chondrocytes were resuspended and filtered through a 40 μm cell filter (Corning, NY, USA) before seeding at a density of 1×10^5 cells/ml in DMEM-F12 medium supplemented with 10% FBS and 1% Penicillin-Streptomycin at 37°C and 5% CO_2. Chondrocytes at passage 2 (P2) were used in our following experiments.

To mimic the dysfunctions of chondrocytes in OA, 10 ng/ml IL-1β (R&D Systems) was used to treat the human chondrocytes for 24 h, and then treated with various concentrations of sEVs or PPD-sEVs for another 48 h. This exposure concentration and duration of IL-1β have been reported to be sufficient to induce abnormality in chondrocytes (Arra et al., 2020).

2.6 | Cellular uptake of PPD-sEVs

DiO staining kit used to label sEVs according to the manufacturer's specifications. Briefly, sEVs and PPD-sEVs were incubated with 10 μM DiO for 30 min in dark at 37°C. Subsequently, the suspension was filtered by 0.22 μm membrane and centrifuged at 100,000g for 140 min to remove the uncombined dye. The purified DiO-labelled sEVs and PPD-sEVs were incubated with chondrocytes for 12 h under 5% CO_2 at 37°C. Then the chondrocytes were fixed with 4% PFA for 25 min and stained with DAPI for 5 min. The images were observed and captured by a confocal microscopy (Leica Microsystems, Wetzlar, Germany). Meanwhile, the DiO staining of PBS only group (PBS group) and DiO co-incubated with PPD group (PPD group) were treated with the same isolation procedure to exclude the possibility of the non-specific labelling of DiO staining. The results were also analyzed by a CytoFLEX flow cytometry (Beckman Coulter, CA, USA) and the DiO-positive sEVs and PPD-sEVs were counted.

2.7 | Cell proliferation assay

A Cell Counting kit-8 (CCK8) kit (Dojindo, Japan) and EdU staining kit were used to evaluate the chondrocyte proliferation according to manufacturers' protocols. For CCK8 assay, human chondrocytes were seeded into 96-well plates at 3000 cells per well. After being incubated with PPD, sEVs, PPD-sEVs for 12, 24, 48, 96 h, the absorbance of chondrocytes in different groups were detected at 450 nm by a spectrophotometer microplate reader. For EdU staining analysis, chondrocytes were incubated with sEVs and PPD-sEVs. Then, 10 μM EdU was added to the DMEM-F12 complete culture medium. Subsequently, the chondrocytes were washed with PBS for three times and fixed with 4% paraformaldehyde (PFA) for 25 min. Chondrocytes in different groups were captured using a confocal microscopy.

2.8 | Chondro-protection of PPD-sEVs to chondrocytes

2.8.1 | Apoptosis Analysis

After treatments, the apoptosis rates of chondrocytes in all groups were detected using an Annexin V-FITC Apoptosis Kit in vitro and then analyzed by a CytoFLEX flow cytometer (Beckman Coulter, CA, USA). In animal studies, the apoptosis rate in each group of mouse cartilage was detected using a TUNEL staining kit.

2.8.2 | Immunofluorescence

Chondrocytes were seeded into six-well plates and cultured in DMEM-F12 complete culture medium. After treated with or without sEVs and PPD-sEVs, chondrocytes in different groups were fixed with 4% PFA for 30 min and then permeabilized with 0.025% Triton-X 100 for 5 min. Subsequently, chondrocytes were blocked with 5% BSA for 30 min and incubated overnight at 4°C with primary antibodies against collagen II (1:1000), aggrecan (1:1000), MMP13 (1:1000), and ADAMTS5 (1:1000). Then, the chondrocytes were incubated with goat-anti-rabbit secondary antibodies labeled with Alexa 488 or Alexa 546 for 60 min followed by 5 min incubation with DAPI for nuclear staining at room temperature. Images in each group were observed and captured by a confocal microscopy.

2.8.3 | Western blot

The protein samples were collected from chondrocyte lysates in different groups using RIPA. The Western Blot analysis were performed as described previously (Gong et al., 2020), after blocked with 5% BSA for 60 min at room temperature to block the unspecific absorption, the PVDF membranes were incubated with primary antibodies including collagen II (1:1000), aggrecan (1:1000), Prg4 (1:1000), MMP13 (1:1000), ADAMTS5 (1:1000), cleaved caspase3 (1:1000), and β-actin (1:1000) overnight at 4°C. Subsequently, the PVDF membranes were incubated with horseradish peroxidase (HRP)-labelled secondary antibody at room temperature for 60 min and chemiluminescent signals were visualized by the ECL Western Blot detection kit and Bio-RAD imaging system.

2.9 | Cartilage uptake, penetration, and retention of PPD-sEVs

All animal experimental procedures were approved by the Animal Research Committee of Shanghai Jiao Tong University Affiliated Sixth People's Hospital (Approval Number: SYXK2011-0128, January 1, 2011, Shanghai, China). Several cartilage explants (Φ 5 mm, 1 mm thickness, 19.14 $\pm$ 0.52 mg) were harvested by an electric drill from the femoral head of pigs. After extraction, the cartilage explants were vigorously washed with PBS containing 1% (v/v) penicillin-streptomycin for 2 h and used immediately after washing. To prepare partially degenerated cartilage explants, several cartilage explants were immersed in 0.1% (w/v) trypsin solution at 37°C for 24 h. Then, the degenerated cartilage explants were vigorously immersed and washed in PBS for three times at 4°C. In order to evaluate the cartilage uptake and penetration capacity of PPD-sEVs or sEVs. sEVs were labelled with a lipophilic fluorescence dye DiI as the procedure described above, and for in vivo imaging study, a near-infrared lipophilic fluorescence dye DiR was used.

The cartilage uptake was measured as the percentage of sEVs from the bath solution to the cartilage explants. And before measurements, the standard curve correlating sEVs concentration and DiI fluorescent intensity was established by a microplate reader. Then the cartilage explants were immersed in 200 μl PBS containing DiI labelled PPD-sEVs or sEVs at 37°C in a 96-well plate for 1, 2, and 4 days. After that, the cartilage explants were removed, and the fluorescent intensity was recorded by the microplate reader.

A self-designed one-way transport Teflon mould was used to evaluate the cartilage penetration of PPD-sEVs or sEVs. The freshly harvested cartilage explants were stuck into the holes in the removable baffle which divided the mould to upper and downstream chamber. Two hundred microlitre suspension of DiI labelled sEVs or PPD-sEVs were added into the upper chamber of the mould, while 200 μl sterilized PBS was added the other chamber of the mould. After penetration for preset time, the cartilage explants of each group were encapsulated with OCT glue and sectioned to 5 μm slides by a vibrating microtome (Leica, Wetzlar, Germany) followed by an immediate confocal microscopy observation.

The intra-articular retention of PPD-sEVs or sEVs was measured by an IVIS Spectrum imaging system (PerkinElmer, USA) in mouse over a period of 21 days. Ten microlitre DiR-labelled sEVs (1×10^{10} particles/ml) was injected to the mouse articular cavity of the right knee, and 10 μl DiR-labeled PPD-sEVs (1×10^{10} particles/ml) was injected to the left knee joint. The images of each mouse joint were recorded by the IVIS Spectrum imaging system at 2 h, 1, 2, 3, 7, 14, and 21 days after intra-articular injection. The data of total radiant efficiency within the region of each knee joint was calculated and presented along with time-based on previous research (B. Geiger, Wang, Padera, Grodzinsky & Hammond, 2018).

2.10 | Evaluation of PPD-sEVs for OA improvement in the ACLT mouse model

2.10.1 Surgical OA model

All animal experimental procedures were approved by the Animal Research Committee of Shanghai Jiao Tong University Affiliated Sixth People's Hospital (Approval Number: SYXK2011-0128, January 1, 2011, Shanghai, China). Sixty eight-week-old male C57BL/six mice underwent sham surgery or anterior cruciate ligament transection (ACLT) surgery were randomly and averagely divided into six groups: (1) Sham group; (2) ACLT + PBS group; (3) ACLT + sEVs (1×10^9 particles/ml) group; (4) ACLT + sEVs (1×10^{10} particles/ml) group; (5) ACLT + PPD-sEVs (1×10^9 particles/ml) group; (6) ACLT + PPD-sEVs (1×10^{10} particles/ml) group. For the ACLT surgery, all mice were anaesthetised with isoflurane and the right knee joints were shaved for aseptic operation. After opening the articular capsule, the anterior cruciate ligament was transected by a micro scissor. Then, sterile saline was used to remove tissue debris by continuous irrigation and the mouse skin incision was closed with sutures. For the sham surgery, the mouse joint was exposed by a medial capsular incision without any other operation, and then the surgical incision was closed. (Jeon et al., 2017). For comparing the cartilage protective effect of sEVs and PPD-sEVs, 10 μl of sEVs (1×10^9 particles/ml; 1×10^{10} particles/ml), PPD-sEVs (1×10^9 particles/ml; 1×10^{10} particles/ml) or PBS was intra-articularly injected into the knee joint cavity of mice by using a 10 μl micro syringe (Hamilton, USA) after two weeks of surgery. In addition, to confirm the reduced injection frequency, sEVs and PPD-sEVs were injected once every two weeks. Six weeks after surgery, all the mice in each group were sacrificed, and the knee joints were harvested for following analysis.

2.10.1 | Histological evaluation and immunohistochemistry

The mouse knee joints in all groups were fixed with 4% PFA for 24 h, and then decalcified with pH = 7.4, 10% EDTA solution at 37°C for two weeks. The decalcified samples were embedded in paraffin and sectioned at 5 μm thickness. The Hematoxylin-Eosin (H&E) Staining Kit was used to examine the cartilage morphology in each group and the Modified Safranin O-Fast Green Cartilage Staining Kit (Solarbio, Beijing, China) was applied to detect the proteoglycan deposition in mice articular cartilage.

According to the previously reported mouse Osteoarthritis Research Society International (OARSI) scoring system (Glasson et al., 2010), the scores of cartilage loss and destruction in all groups were calculated. For immunohistochemistry analysis, cartilage sections in each group were deparaffinized in xylene, hydrated through ethanol series and then repaired by using pepsin antigen repair solution (Solarbio, Beijing, China). Subsequently, all the sections were blocked with 5% BSA for 30 min and incubated with primary antibodies against collagen II (1:100), aggrecan (1:100), MMP13 (1:200), ADAMTS5 (1:200), IL-1β (1:100), TNFα (1:100), and NGF (1:100) overnight at 4°C. Then each section was incubated with the HRP-labelled secondary antibodies for 60 min, and 3-amino-9-ethylcarbazole (AEC) Peroxidase Substrate Kit (Solarbio, Beijing, China) or DAB (Servicebio, Wuhan, China) was used as HRP-specific substrate. The images were observed and captured by a light microscopy (Leica Microsystems, Wetzlar, Germany). The positive rate (%) of each marker in each group was calculated, and then the fold change of each marker in each group was normalized against the Sham group (vs. Sham group).

2.10.2 | Pain measurements

Reflexive measures of pain using stimulus-evoked responses, such as hind-paw withdrawal threshold, are commonly used to assess OA-related pain (Wei et al., 2021). Hind-paw withdrawal thresholds were measured according to a previous report (Huang et al., 2019). Briefly, the mice were placed individually in an elevated metal grid cage with sufficient space for them to move their paws while the rest of their body was restricted with plastic plates. After the mice acclimated to the apparatus, the mouse's right hind-paw withdrawal threshold was evaluated by using an electronic von Frey instrument (model BIO-EVF4; Bioseb, Vitrolles France). The probe tip of the instrument was gently placed perpendicularly into the mid-plantar surface of the paw, and steadily increasing pressure (between 0 and 100 grams) was applied until the hind paw was first lifted. This force is independent of the movements of the limb. The hind-paw withdrawal threshold was recorded as the required pressure to first lift the paw. The data were expressed as withdrawal threshold in grams (g). Lower withdrawal threshold values (g) were taken as indicators of pain.

2.11 | Statistical analysis

All experiments were repeated at least three times independently and expressed as mean $\pm$ standard deviation (S.D.). The Student's t-test was applied for comparison between two groups. One-way analysis of variance (ANOVA) was performed for comparisons among various groups. Statistical analyses were carried out by using GraphPad Prism 8 software (CA, USA). Statistical significance was set as $P < 0.01$ (**) and $P < 0.05$ (*).

3 | RESULTS

3.1 | Reversing the surface charge of iMSC-sEVs by PPD modification

To reverse the surface charge of iMSC-sEVs (sEVs), a cationic amphiphilic macromolecule PPD was designed based on εPL and DSPE-PEG (Figure 1A). Charateristic peaks of εPL and DSPE-PEG were found in the ^{1}H-NMR spectrum of PPD, and about 4% lysine units were conjugated to DSPE-PEG as calculating from the peak integration value of -CH$_3$ in DSPE-PEG and α-H in εPL (Figure 1B). Furthermore, MOLDI-TOF results showed an about 2 KDa increasment of the molecular weight of PPD ($\sim$6.8 KDa) to that of εPL (Figure S1), suggesting that about one molecule of PEG-DSPE was grafted to a εPL molecule on average. In addition, PPD was cytocompatible as there was no difference between the proliferation of human chondrocytes cultured with medium containing 100 μg/ml PPD and with normal culture medium (control group, Figure 1C).

Then, the ability of PPD in modifying sEVs to reverse the negative surface charge was evaluated. First, the positive modification rate of PPD to sEVs was detected to assess the binding ability. Nano-flow cytometry (NFC) results (Figures 2A and S2A) showed that PPD could successfully modify sEVs with a dose-dependent manner below 100 μg/ml as increasing PPD concentration could lead to an increased modification rate. While, there is no significant difference in PPD modification rate among 100, 200, and 400 μg/ml groups (Figure S2B). After the confirmation of successful PPD modification to sEVs, the zeta potential of PPD-sEVs was analyzed. The average zeta potential of the original sEVs was -17.89 $\pm$ 2.85 mV. While, PPD (100 μg/ml) modified sEVs (PPD-sEVs) presented an average zeta potential of 8.26 $\pm$ 1.62 mV, demonstrating the successful surface charge reverse of sEVs (Figure 2B). In addition, the average zeta potential of PPD-sEVs prepared by incubating sEVs with 100, 200, or 400 μg/ml PPD suspensions exhibited no significant difference. Thus, 100 μg/ml PPD concentration was chosen to prepare PPD-sEVs in the following study. Then, the average size of PPD-sEVs were evaluated to identify the preserve of the physiochemical properties of sEVs after PPD modification. As shown in Figure 2C, the average diameter of PPD-sEVs was 76.27 $\pm$ 5.01 nm and showed no statistical difference in comparison with that of the unmodified sEVs (73.83 $\pm$ 5.63 nm). A typical cup-shaped morphology like unmodified sEVs was presented in the transmission electron microscopy (TEM) image of PPD-sEVs (Figure 2D). The round
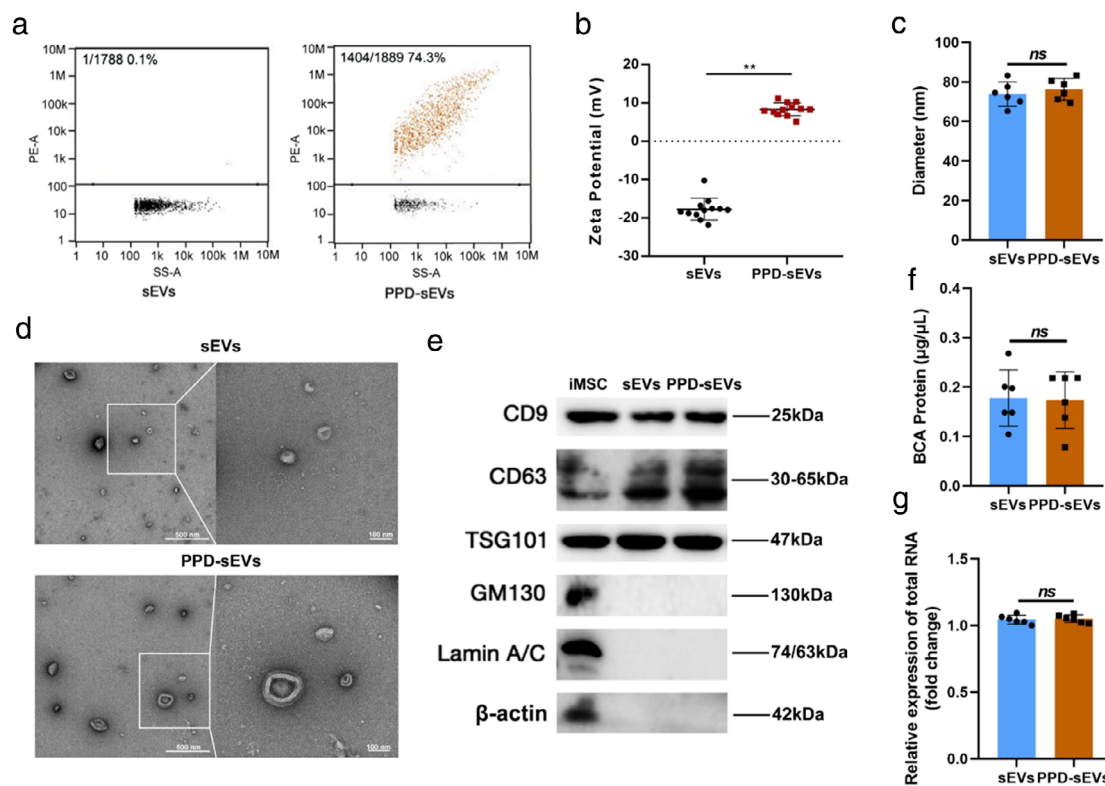
FIGURE 2 Characterization of PPD-sEVs. (A) The PPD modification rate of sEVs incubating with 100 μg/ml PPD suspension. RITC labeled PPD (100 μg/ml) was incubated with sEVs (1×10^{10} particle/ml), and PPD-sEVs were isolated by ultracentrifugation before detected by a nano-flow cytometry; (B) Zeta potential of sEVs and PPD-sEVs ($n = 12$); (C) Average particle diameter of sEVs and PPD-sEVs measured and analyzed by a nano-flow cytometry; (D) Representative TEM image of PPD-sEVs or sEVs, scale bar: 500 and 100 nm; (E) Western Blot analysis of CD9, CD63, TSG101, GM130, Lamin A/C, and β-actin from iMSC, sEVs, and PPD-sEVs. CD9, CD63, and TSG101: sEVs specific marker; GM130: The Golgi marker; Lamin A/C: Nuclear marker; β-actin: Cytoskeletal marker; (F) The protein concentration of sEVs and PPD-sEVs were detected by BCA assay ($n = 6$); (G) Total RNA amounts in sEVs and PPD-sEVs group were analyzed by using the RNA dye SYTO to label sEVs RNA ($n = 6$) **$P < 0.01$

spherical shape with double-layer membrane structure of the sEVs and PPD-sEVs was observed by cryo-TEM analysis (Figure S3). Moreover, no sign of sEVs aggregation or PPD aggregating contaminant (Figure S4A, the morphology of PPD micelles) was observed in the TEM image of PPD-sEVs. In addition, to further examine the possible containments of soluble PPD or aggregating PPD, 100 μg/ml RITC labelled PPD was treated as the procedure for PPD-sEVs isolation. After ultracentrifugation, no fluorescent signal could be detected in the resuspension solution that rinsed the tube bottom (Figure S4B), excluding the containments of soluble or aggregating PPD during PPD-sEVs isolation.

The therapeutic functions of MSC-sEVs are mainly dependent on their cargos like proteins and RNAs, and thus maintenance of these cargos after PPD modification is quite important. Thus, we evaluated the impact of PPD modification on the internal cargos of sEVs. BCA assay was used to evaluate the change of total proteins, and PPD generated no background signal in BCA test (Figure S5A). As shown in Figure 2F, compared with the unmodified sEVs, no significant change in the total protein content of PPD-sEVs (Figure S5A) was detected. Further Western Blot analysis results of six selected internal proteins of sEVs also revealed the similar trend (Figure S5B). Furthermore, the total RNA amounts (Figure 2G) quantified by RNA fluorescent dye were nearly unchanged after PPD modification. The qPCR results of six selected microRNAs (Figure S5C–H) also showed no statistical difference between sEVs group and PPD-sEVs group. These results demonstrated that PPD modification did not significantly change the cargo contents of sEVs. In addition, some proteins on the sEVs surface such as CD73 also contribute to the bioactivity of MSC-sEVs (Witwer et al., 2019; Zhang et al., 2018). Therefore, to rule out the possibility of the disturbance on surface functional proteins of sEVs after PPD modification, the expression of CD73 was detected in sEVs and PPD-sEVs, and downstream Akt pathway related proteins, including total Akt, p-Akt, total Erk, and p-Erk, were analyzed in chondrocytes after sEVs or PPD-sEVs treatment. Our results demonstrated that PPD modification had no influence on the expression of CD73 (Figure S6A) and downstream Akt pathway related proteins (Figure S6B).

Collectively, all these results prove that PPD modification can reverse the surface charge of sEVs without changing the typical physiochemical properties and contents of sEVs.
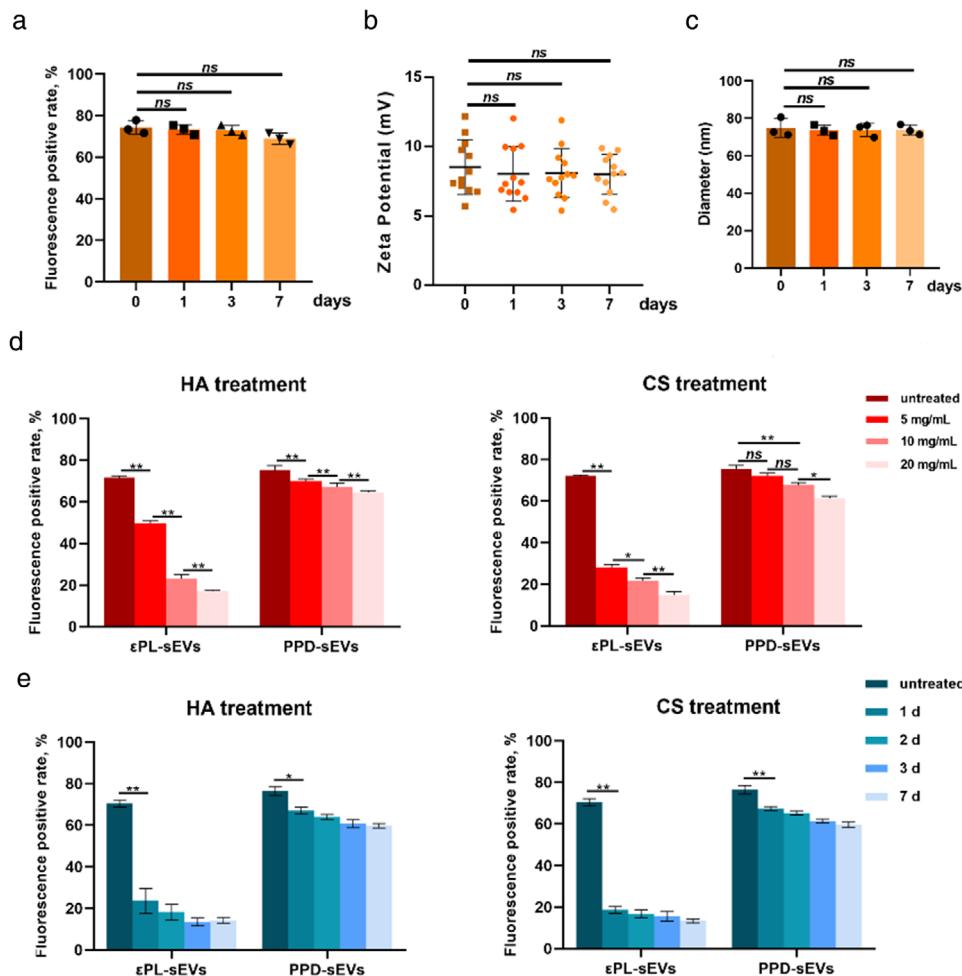
FIGURE 3 The stability of PPD modified sEVs. (A) The change of PPD modification rate in a 7-day period ($n = 3$); (B) The zeta potential of PPD-sEVs was detected in a 7-day period ($n = 12$); (C) The average particle diameter of PPD-sEVs was in a 7-day period ($n = 3$); (D) The PPD modification rate after 1-day incubation with various concentration of HA (Mw 100 KDa) or CS (50 KDa) solutions (0, 5, 10, 20 mg/ml); (E) PPD modification stability under the interference of 10 mg/ml HA or CS in a 7-day period ($n = 3$) *$P < 0.05$, **$P < 0.01$

3.2 | Characterization of the PPD modification stability

Next, the PPD modificaiton rate, zeta potential, and average size of PPD-sEVs were monitored for a 7-day period to evaluate their colloidal stability. The fluorescence positive rate (Figure 3A), zeta potential (Figure 3B), and average diameter (Figure 3C) of PPD-sEVs presented no statistical difference between the 0-d group and other groups, which means PPD-sEVs presented a good stability in PBS solution.

Anionic biomacromolecules like HA and CS distribute widely in the joint cavity and cartilage matrix. However, these negatively charged macromolecules can compete with the negatively charged surface of sEVs to bind PPD by electrostatic interaction, leading to the detachment of PPD from sEVs and modification failure. Therefore, the PPD modification stability under the presence of HA or CS was evaluated, and the change of PPD modification rate was chosen as an indicator for modification stability. In addition, εPL modified sEVs (εPL-sEVs) were used as a control group, because εPL could only bind sEVs by electrostatic interaction. Figure S7 showed that sEVs could also be modified by 100 μg/ml εPL with a modification rate of 70.5%. However, the modification rate of εPL-sEVs decreased dramatically after incubation with increasing concentrations of HA and CS for 24 h (Figure 3D). Meanwhile, only a minor decrease in modification rate was detected in PPD-sEVs incubated with all concentrations of HA and CS. Furthermore, as shown in Figure 3E and Table S3, about 60% PPD modification rate was kept for PPD-sEVs after incubation with 10 mg/ml HA (59.7% $\pm$ 1.06%) or 10 mg/ml CS (59.57% $\pm$ 1.29%) for 7 day. However, the modification rate of εPL-sEVs decreased dramatically after 1 day incubation (23.7% $\pm$ 5.96% for HA group and 18.67% $\pm$ 1.68% for CS group), and less than 15% εPL-sEVs were detected 7 day later. These results proved a stable PPD modification to the bilayer lipid membrane of sEVs under anionic macromolecule interference and a successful self-assembly of PPD on the bilayer lipid membrane.
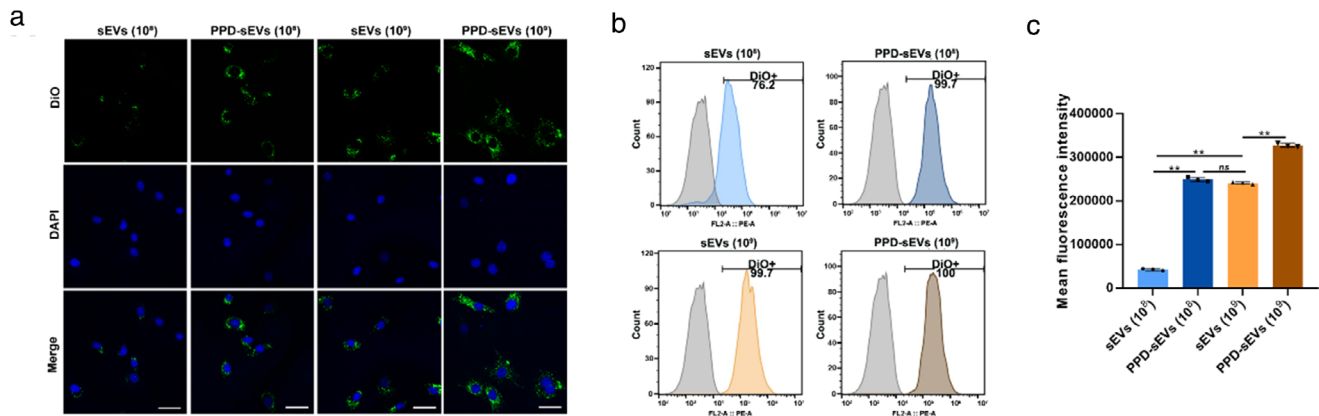
FIGURE 4 Chondrocyte uptake of PPD-sEVs. (A) Representative images of the chondrocyte uptake of DiO (Green) labelled sEVs or PPD-sEVs, scale bar: 50 μm; (B) Positive chondrocyte rate for uptake of DiO labled sEVs or PPD-sEVs; (C) Mean fluorescence intensity (MFI) of DiO-labelled sEVs and PPD-sEVs in each group ($n = 3$) **$P < 0.01$

3.3 | Cellular uptake and chondrocyte modulation ability of PPD-sEVs

Preserving the function of sEVs after PPD modification is very critical for their further application in OA modulation. And the foundation of sEVs based therapy is the successful delivery of their cargo to target cells. Thus, the cellular uptake of PPD-sEVs on cultured human chondrocytes was investigated. First, we confirmed that nearly no DiO signal was detected inside chondrocytes that were incubated with the PBS resuspensions of 10 μg/ml DiO solution in PBS or PBS with 100 μg/ml PPD solution after the same isolation procedures in PPD-sEVs group, excluding the possible interference of DiO cluster (Figure S8). The fluorescent images of chondrocyte uptake showed that PPD-sEVs displayed a better cellular uptake capacity than unmodified sEVs (Figure 4A) at both particle concentrations. Furthermore, flow cytometry analysis further revealed a higher positive rate of PPD-sEVs treated chondrocytes in comparison with that of sEVs treated chondrocytes at the particle concentration of 1×10^8 particles/ml (Figure 4B). A similar positive rate between 1×10^9 particles/ml sEVs group and 1×10^9 particles/ml PPD-sEVs group were observed, but the mean fluorescence intensity (MFI) of 1×10^9 particles/ml PPD-sEVs treated group was significantly higher than that of 1×10^9 particles/ml sEVs treated group (Figure 4C), manifesting an enhanced chondrocyte uptake capacity of PPD-sEVs.

As the improved cellular uptake efficacy might enhance the chondrocyte modulation ability of sEVs, the chondrocyte modulation functions of PPD-sEVs were further studied using an in vitro IL-1β induced model where the homeostasis of chondrocyte was destroyed. After being cultured with PPD-sEVs or sEVs under 10 ng/ml IL-1β for 48 h, the proliferation of chondrocytes in 1×10^8 particles/ml sEVs treated group and only IL-1β treated group showed no significant difference. By contrast, 1×10^8 particles/ml PPD-sEVs could promote the proliferation of chondorcytes as the absorbance of chondrocytes treated with 1×10^8 particles/ml PPD-sEVs was 1.16-fold higher (with significant difference) than that of chondrocytes treated with 1×10^8 particles/ml sEVs (Figure 5A). The EdU staining results were in accordance with CCK8 assay, demonstrating the enhanced function of PPD-sEVs to chondrocyte proliferation (Figure 5B,C). Then, the anti-apoptotic effects of sEVs and PPD-sEVs on IL-1β treated chondrocytes was analyzed by Annexin V-FITC/PI staining and flow cytometry. As shown in Figure 5D,E, 1×10^8 particles/ml sEVs had no obvious influence on the IL-1β induced apoptosis, while 1×10^8 particles/ml PPD-sEVs could partially decreased the percentage of apoptotic chondrocytes (from 47.86% to 21.45%). Moreover, 1×10^9 particles/ml PPD-sEVs (9.83% apoptotic cells) displayed greater chondro-protective effect as compared with 1×10^9 particles/ml sEVs (24.61% apoptotic cells). Meanwhile, Western Blot analysis of an apoptosis-related marker cleaved caspase3 revealed similar results (Figure 5F). Given the essential role of ECM metabolism homeostasis in mediating OA cartilage repair and regeneration, anabolism (collagen II, aggrecan) and catabolism (MMP13, ADAMTS5) markers in chondrocytes were detected by immunofluorescence microscopy and the results are shown in Figures 5G and S9. 1×10^8 particles/ml sEVs failed to modulate the metabolism of chondrocytes, but 1×10^8 particles/ml PPD-sEVs partially reversed the imbalance of metabolism homeostasis. And 1×10^9 particles/ml PPD-sEVs group displayed more fluorescence positive rates of collagen II (1.538-fold) and aggrecan (1.376-fold) and less fluorescence positive rates of MMP13 (0.657-fold) and ADAMTS5 (0.628-fold) than 1×10^9 particles/ml sEVs group (Figure S9). The results in Western Blot analysis (Figure 5F) were consistent with the microscope observation, demonstrating that PPD-sEVs could restore the chondrocyte homeostasis more effectively than original sEVs.
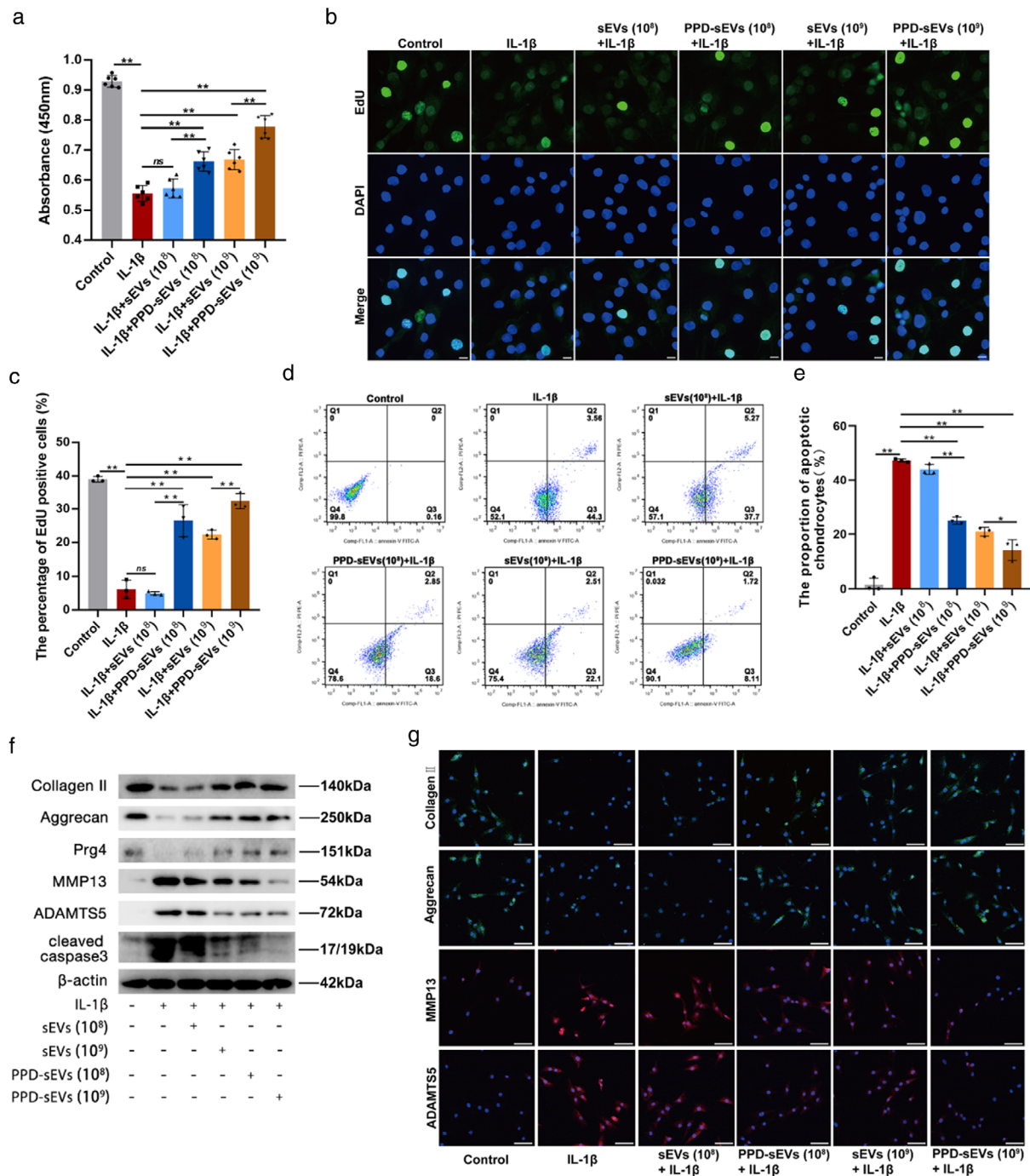
FIGURE 5 In vitro chondrocyte homeostasis modulation capacity of PPD-sEVs. (A) The chondrocyte proliferation in each group detected by CCK8 assay ($n = 6$); (B) Representative EdU staining images of PPD-sEVs or sEVs treated groups, scale bar: 10 μm; (C) Statistical evaluation of fluorescent intensity after EdU staining ($n = 3$); (D, E) Chondrocyte apoptotic levels detected by flow cytometry assay and results ($n = 3$); (F) Western Blot analysis of chondrocyte anabolism related markers (Collagen II, Aggrecan, Prg4), catabolism related markers (ADAMTS5, MMP13), and apoptosis related marker (cleaved caspase3); (G) Immunofluorescence staining of cartilage matrix anabolism (Collagen II, Aggrecan; Green) and catabolism (ADAMTS5, MMP13; Red) related biomarkers in each group, scale bar: 100 μm. *$P < 0.05$, **$P < 0.01$

3.4 | Uptake, penetration, and retention of PPD-sEVs in cartilage

Considering the distribution of abundant anionic components in cartilage matrix, we hypothesized that PPD modification can improve the uptake, penetration, and retention of sEVs in cartilage. Therefore, the above capacities of PPD-sEVs were explored. For the uptake evaluation, cartilage explants (Φ 5 × 1 mm, 19.14 ± 0.52 mg) extracted from pig joints were incubated with DiI
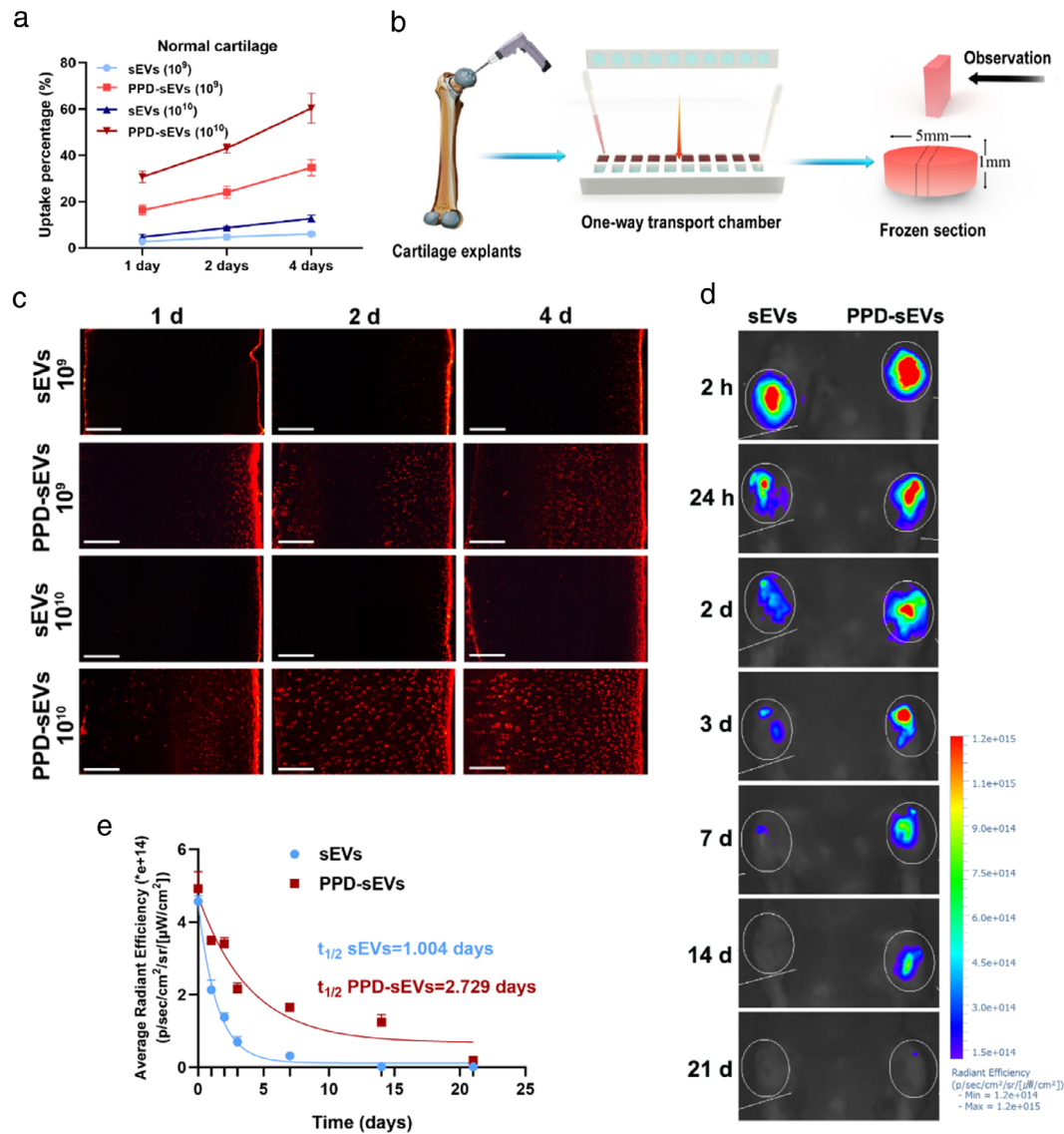
FIGURE 6 Enhanced cartilage uptake, penetration, and retention capacity of PPD-sEVs. (A) Cartilage uptake percentages of DiI labelled sEVs or PPD-sEVs in cartilage explants from pig for a 4-day period, $n = 3$; (B) Schematic illustration of penetration assay; (C) Microscope images of DiI (Red) labelled sEVs or PPD-sEVs across the diffusion gradient (right to left) of normal cartilage, scale bar: 200 μm; (D) Representative IVIS images of mice injected with DiR labelled sEVs or PPD-sEVs over 21 days after intraarticular injection; (E) Time course of fluorescent radiant efficiency within joints in sEVs and PPD-sEVs group. Data are fit to a one-phase exponential decay with a common plateau based on background signal ($n = 3$). Half-lives were statistically different for each dataset ($P < 0.0001$) by extra sum of squares F-test

labelled PPD-sEVs or sEVs, and the cartilage uptake was measured as the percentage of sEVs from 200 μl suspension to the cartilage explants. First, we detected the DiI labelling stability of sEVs for a 21-day period in vitro, and it showed no statistical difference between the 0-day group and the 21-day group (Figure S10), which means a stable labelling of DiI to sEVs. The results in Figure 6A and Table S4 showed that the cartilage uptake of both PPD-sEVs and sEVs were enhanced with the increasing sEVs concentrations. Obviously, PPD-sEVs exhibited significantly higher cartilage uptake percentage and absorbed rate than unmodified sEVs at all time points. For example, 24 h later, 16.4% $\pm$ 1.95% (1×10^9 particles/ml) and 30.67% $\pm$ 2.26% (1×10^{10} particles/ml) PPD-sEVs were taken in by cartilage explants while it was only 2.77% $\pm$ 0.67% (1×10^9 particles/ml) and 4.67% $\pm$ 1.10% (1×10^{10} particles/ml) for unmodified sEVs. Cartilage matrix degradation is a major pathological manifestation of OA. Our results (Figure S11A) also revealed a promoted uptake percentage of both PPD-sEVs and sEVs in partially degenerated cartilage explants.

For the evaluation of cartilage penetration ability, cartilage explants were stuck and sealed in a self-designed one-way transport chamber made of Teflon, and 200 μl DiI labelled PPD-sEVs or sEVs suspensions were added to the upper chamber and PBS were added to the lower chamber (Figure 6B). After penetration for 1, 2, and 4 day at 37°C in a sterile incubator, the cartilage explants were sectioned and imaged by laser confocal microscopy. As shown in Figure 6C, unmodified sEVs still concentrated in the

superficial layer of the cartilage explants in both concentrations, and very limited penetration distance was exhibited in 4 day. As a contrast, PPD-sEVs at the concentration of 1×10^9 particles/ml had diffused into the middle layer of cartilage explants in 2 day. Furthermore, it is worth noting that 1×10^{10} particles/ml PPD-sEVs had distributed throughout the cartilage explants after 2 day penetration. In addition, a promoted penetration of both PPD-sEVs and sEVs was also proved in partially degenerated cartilage explants (Figure S11B). All these results demonstrated an improved cartilage penetration ability of PPD-sEVs.

In vivo imaging analysis was used to further analyze the joint retention ability of PPD-sEVs. First, we excluded the possible fluorescent signal of DiR cluster in the joint space (Figure S12). Next, the DiR-labeled PPD-sEVs or sEVs (1×10^{10} particles/ml) were injected into left or right knee joint cavity respectively. For a 21-day period, DiR fluorescence signal in the bilateral knee were serially detected and calculated. Twenty-four hours after the intra-articular injection, we detected bright fluorescence signals in PPD-sEVs group and sEVs group (Figure 6D). However, the fluorescence signals were decreased dramatically 3 day after sEVs injection, while PPD-sEVs injection group showed obviously slower reduction in fluorescence intensity during the same period. Surprisingly, the DiR fluorescence signals were still detectable in PPD-sEVs group at 14 and 21 day after intra-articular injection, while the fluorescence signals were totally disappeared in sEVs group 14 day after injection. Applying the data in two groups to a single-phase exponential decay function, we found that the unmodified sEVs had a joint half-life of only 1.004 days, whereas PPD-sEVs significantly prolonged the half-life to 2.729 days (Figure 6E). These results demonstrated that PPD-sEVs showed significantly extended joint retention ability.

3.5 | Enhanced efficacy of PPD-sEVs for OA improvement in the ACLT model of mouse

PPD-sEVs not only exhibited enhanced chondro-protective effect in vitro, but also displayed an improved cartilage uptake, penetration, and retention ability in contrast with sEVs. Then, we investigated whether the advanced features of PPD-sEVs can improve the bioavailability of sEVs for OA treatment in a well-established ACLT model of mouse. Fourteen days after ACLT surgery, 10 μl PPD-sEVs, sEVs, or PBS were intra-articularly injected into the right knee joint of the mice weekly (Figure 7A). Four weeks later, Hematoxylin-Eosin (H&E) staining and Safranin O-Fast Green (Safranin O) staining were performed to evaluate the cartilage degeneration in each group. As shown in Figure 7B, obvious cartilage degeneration and abrasion presented in the representative image of PBS treated group, and those features were also found in 1×10^9 particles/ml sEVs treated group. By contrast, the images of 1×10^9 particles/ml PPD-sEVs, 1×10^{10} particles/ml sEVs, or 1×10^{10} particles/ml PPD-sEVs treated groups showed relatively low degree of those signs.

Histological analysis was applied to quantify the severity of OA in a blinded manner according to the OARSI scoring system (Glasson et al., 2010). As shown in Figure 7C, there was no significant difference between the OARSI scores between 1×10^9 particles/ml PPD-sEVs (P = 3.67 ± 0.49) treated group and PBS treated group (4.67 ± 0.49, P = 0.97). While, the score of 1×10^9 particles/ml PPD-sEVs treated group was significantly lower than that of 1×10^9 particles/ml sEVs treated group. In addition, both 1×10^{10} particles/ml PPD-sEVs or sEVs treated group showed significantly lower scores than that of PBS treated group. The results in Figure 4 indicated that PPD-sEVs could efficiently modulate the imbalance of chondrocyte homeostasis. Then, immunohistochemistry (IHC) staining of metabolism-related protein was carried out to verify whether PPD-sEVs had similar function in ACLT-induced mice. IHC staining results (Figure 7D–H) manifested that the levels of anabolism related markers (collagen II, aggrecan) were increased and catabolism related markers (MMP13, ADAMTS5) were decreased in ACLT-induced mice after the treatment of 1×10^9 particles/ml PPD-sEVs, while sEVs with the same concentration showed no significant difference to PBS injection group. Meanwhile, both of PPD-sEVs and sEVs at 1×10^9 particles/ml could effectively maintain the homeostasis between cartilage anabolism and catabolism in OA mice. Both 1×10^9 particles/ml and 1×10^{10} particles/ml PPD-sEVs and sEVs can successfully modulate the homeostasis of cartilage in OA. In addition, the anti-apoptotic results of PPD-sEVs and sEVs in articular cartilage of ACLT-induced mice were detected and analyzed by TUNEL staining as shown in Figure 7I,J. Both 1×10^9 particles/ml and 1×10^{10} particles/ml sEVs or PPD-sEVs could decrease the apoptotic levels of chondrocytes, while 1×10^9 particles/ml PPD-sEVs showed a better anti-apoptotic effect than 1×10^9 particles/ml sEVs, and 1×10^{10} particles/ml PPD-sEVs showed no significant difference to 1×10^{10} particles/ml sEVs group in OA mice.

Frequent intra-articular injections brought some problems, such as infection and soft tissue injuries. Therefore, reducing the injection frequency is critical for the clinical application of MSC-sEVs for OA. In consideration of the prolonged retention ability of PPD-sEVs, biweekly injection of PPD-sEVs or sEVs was also conducted in the study (Figure 8A). The results in Figure 8B,C indicated that biweekly injection of 1×10^{10} particles/ml PPD-sEVs could also effectively alleviate cartilage destruction. While, the mice in 1×10^{10} particles/ml sEVs injection group exhibited more severe OA features than those in 1×10^{10} particles/ml PPD-sEVs treatment group. In addition, we also found that biweekly injection of 1×10^9 particles/ml PPD-sEVs or sEVs could not induce significant modulation to OA. IHC results further demonstrated that the expressions of cartilage matrix anabolism-related markers (collagen II, aggrecan) were up-regulated, and catabolism-related proteins (MMP13, ADAMTS5) were down-regulated after the injection of 1×10^{10} particles/ml PPD-sEVs in OA mice (Figure 8D–H). However, there was no significant improvement on the expression of collagen II and aggrecan or obvious inhibition on the expression of MMP13 and ADAMTS5 in 1×10^{10} particles/ml sEVs treatment group. Furthermore, the biweekly administration of 1×10^{10} particles/ml PPD-sEVs could significantly decrease
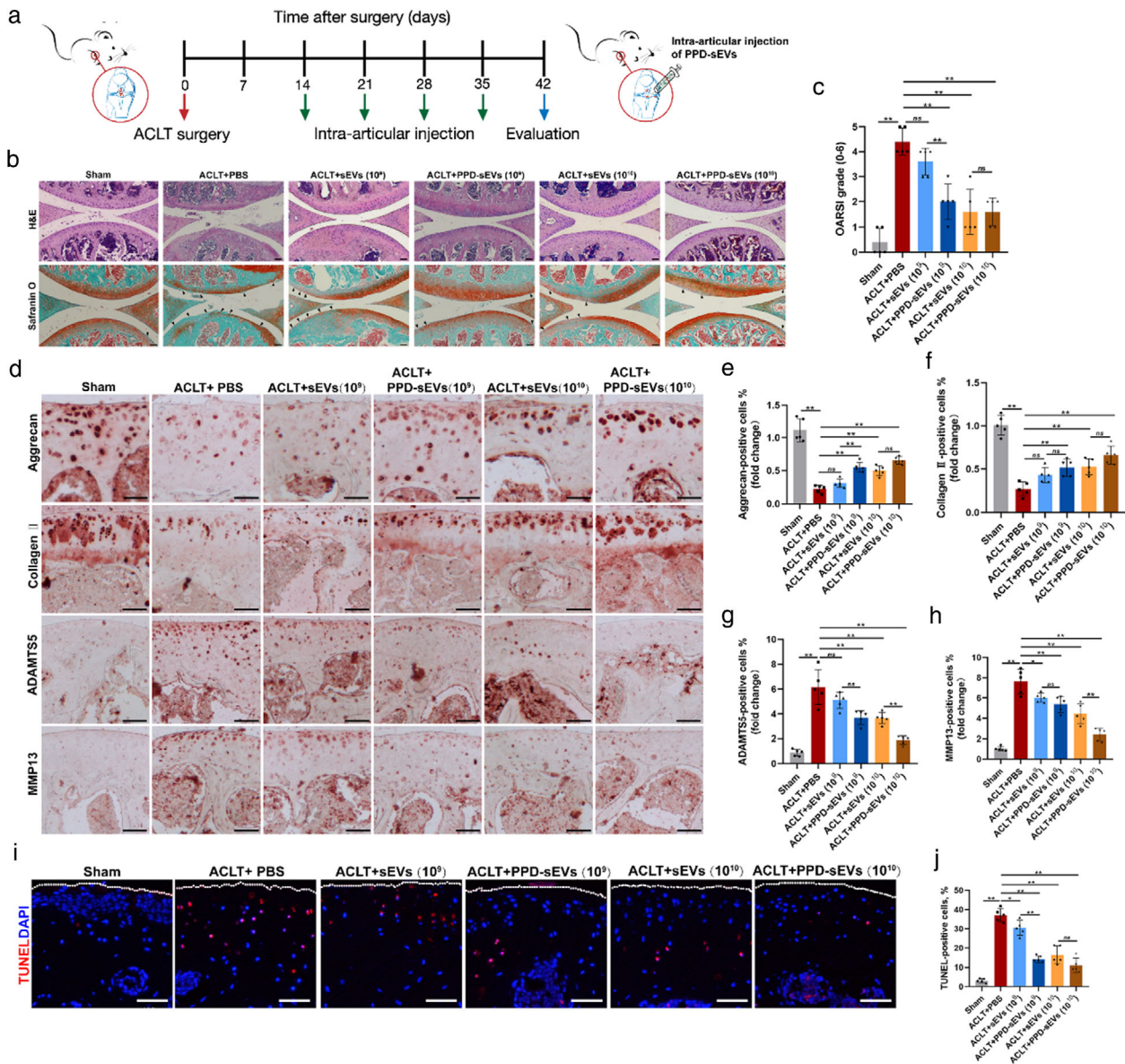
FIGURE 7 In vivo evaluation of PPD-sEVs for OA improvement in the ACLT mouse model. (A) Schematic illustration of ACLT surgery, sEVs intra-articular injection, and cartilage harvest timeline; (B) Representative images of H&E and Safranin O-Fast Green (Safranin O) staining. Black triangles indicate cartilage loss and destruction, scale bar: 200 μm; (C) Statistic data of OARSI scores in each group ($n = 5$); (D) Representative images of immunohistochemistry analysis for cartilage matrix anabolism biomarkers (Aggrecan, Collagen II) and catabolism biomarkers (ADAMTS5, MMP13) in each group, scale bar: 100 μm; (E, F) Quantitative analysis of immunohistochemical staining of cartilage matrix anabolism biomarkers (Aggrecan, Collagen II) ($n = 5$); (G, H) Quantitative analysis of immunohistochemical staining of cartilage matrix catabolism biomarkers (ADAMTS5, MMP13) ($n = 5$). The fold change of each marker in each group was normalized against the Sham group (vs. Sham group); (I) Representative images of TUNEL staining analysis to detect chondrocyte apoptosis (Red) in articular cartilage in different groups, scale bar, 100 μm; (J) Quantitative analysis of apoptotic chondrocytes in each group ($n = 5$), scale bar, 100 μm. *$P < 0.05$, **$P < 0.01$

the TUNEL-positive rate of chondrocytes, while 1×10^{10} particles/ml sEVs treatment showed no statistically difference to the PBS group (Figure 8I,J). Moreover, as the pain relief is an important aspect of OA management, we examined pain recovery in each group by hind-paw withdrawal thresholds analysis and IHC staining of pain-related inflammatory markers (IL-1β, TNFα, NGF). Our results showed biweekly injection of PPD-sEVs (1×10^{10} particles/ml) could effectively relieve OA-related pain as withdrawal threshold (Figure 9A) was raised from 23.8 ± 8.42 g to 42.4 ± 7.94 g. In addition, compared with 1×10^{10} particles/ml sEVs group (26.6 ± 8.06 g), an obvious increasement in the withdrawal threshold was observed in 1×10^{10} particles/ml PPD-sEVs group, but there is no statistical difference between sEVs treated group and PPD-sEVs treated group ($P = 0.0946$). Furthermore, the expressions of inflammatory factors were decreased after 1×10^{10} particles/ml PPD-sEVs treatment (Figure 9B–E). However, all the other treatment groups failed in significantly relieving the pain or downregulating the expressions of inflammatory marker.
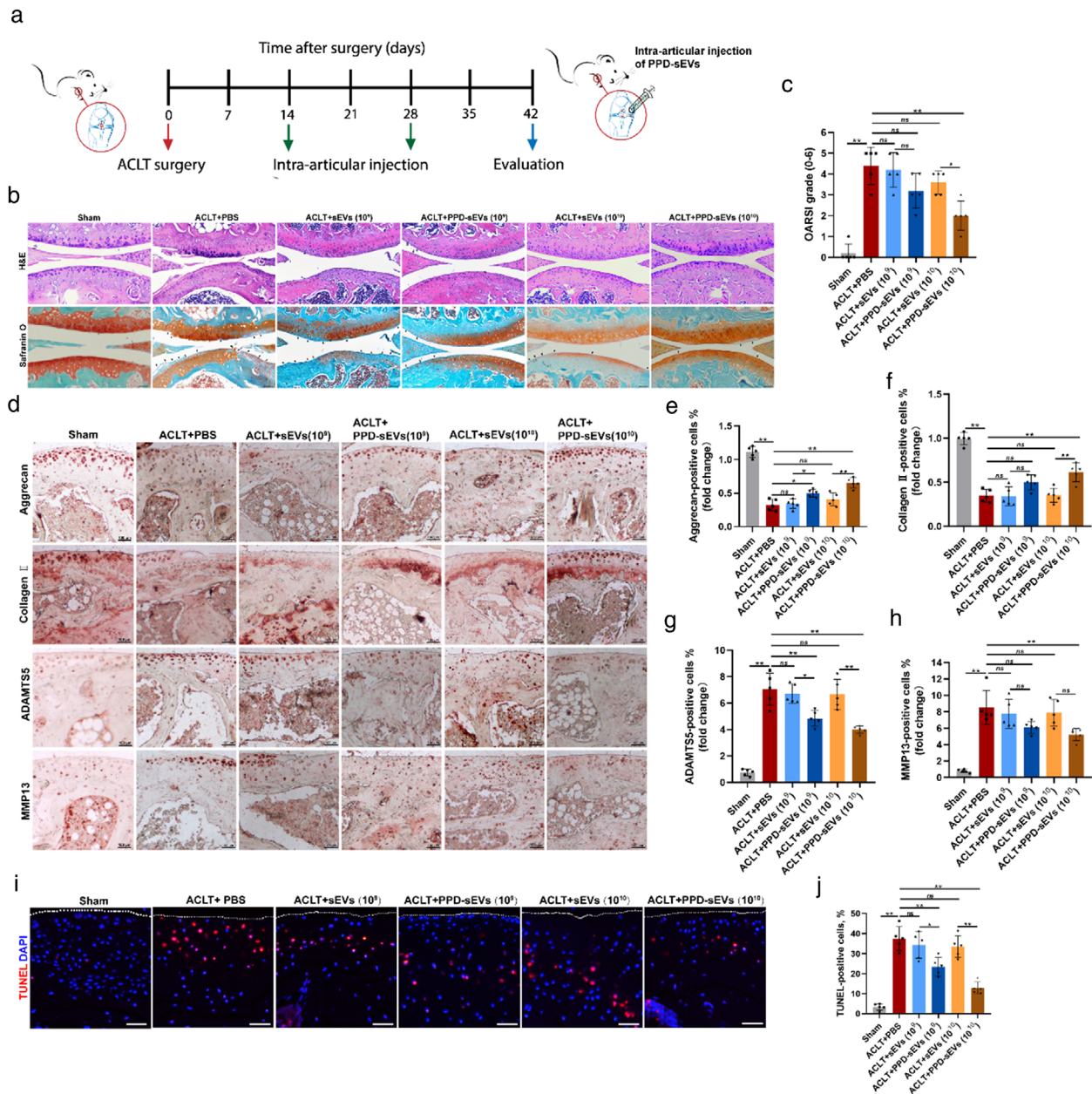
FIGURE 8 **Reduced injection frequency of PPD-sEVs for OA improvement**. (A) Schematic illustration of processing timeline and procedures; (B) Representative H&E and Safranin O-Fast Green (Safranin O) staining images in each group. Black triangles indicate cartilage loss and destruction, scale bar: 200 μm; (C) Statistic data of OARSI scores in each group ($n = 5$); (D) Representative images of immunohistochemistry analysis for cartilage matrix anabolism biomarkers (Aggrecan, Collagen II) and catabolism biomarkers (ADAMTS5, MMP13) in each group, scale bar: 100 μm; (E, F) Quantitative analysis of immunohistochemical staining of Aggrecan and Collagen II ($n = 5$); (G, H) Quantitative analysis of immunohistochemical staining of ADAMTS5 and MMP13 ($n = 5$), the fold change of each marker in each group was normalized against the Sham group (vs. Sham group); (I, J) Detection of TUNEL-positive (Red) chondrocytes in articular cartilage by TUNEL staining and the statistical results ($n = 5$), scale bar, 100 μm. *$P < 0.05$, **$P < 0.01$

4 | DISCUSSION

The function of MSC-sEVs in modulating cartilage homeostasis and inflammation indicate their potential as disease modifying factors for OA treatment. However, the low intra-articular bioavailability of MSC-sEVs mainly caused by the cartilage matrix hinderance effect severely impedes their future clinical applications. To overcome the hinderance, a surface charge reversing strategy of MSC-sEVs is raised in this study for OA treatment for the first time.

Delivery of the loading bioactive factors to cartilage is essential for MSC-sEVs based OA therapy, which requires effective biodistribution of intra-articularly injected sEVs in cartilage tissue (K. H. Kim, Jo, et al., 2020; Mancuso et al., 2019). The cartilage distribution of the solutes in synovial fluid was depends on two competing rates, namely the cartilage entering rate N_{Entry} and the
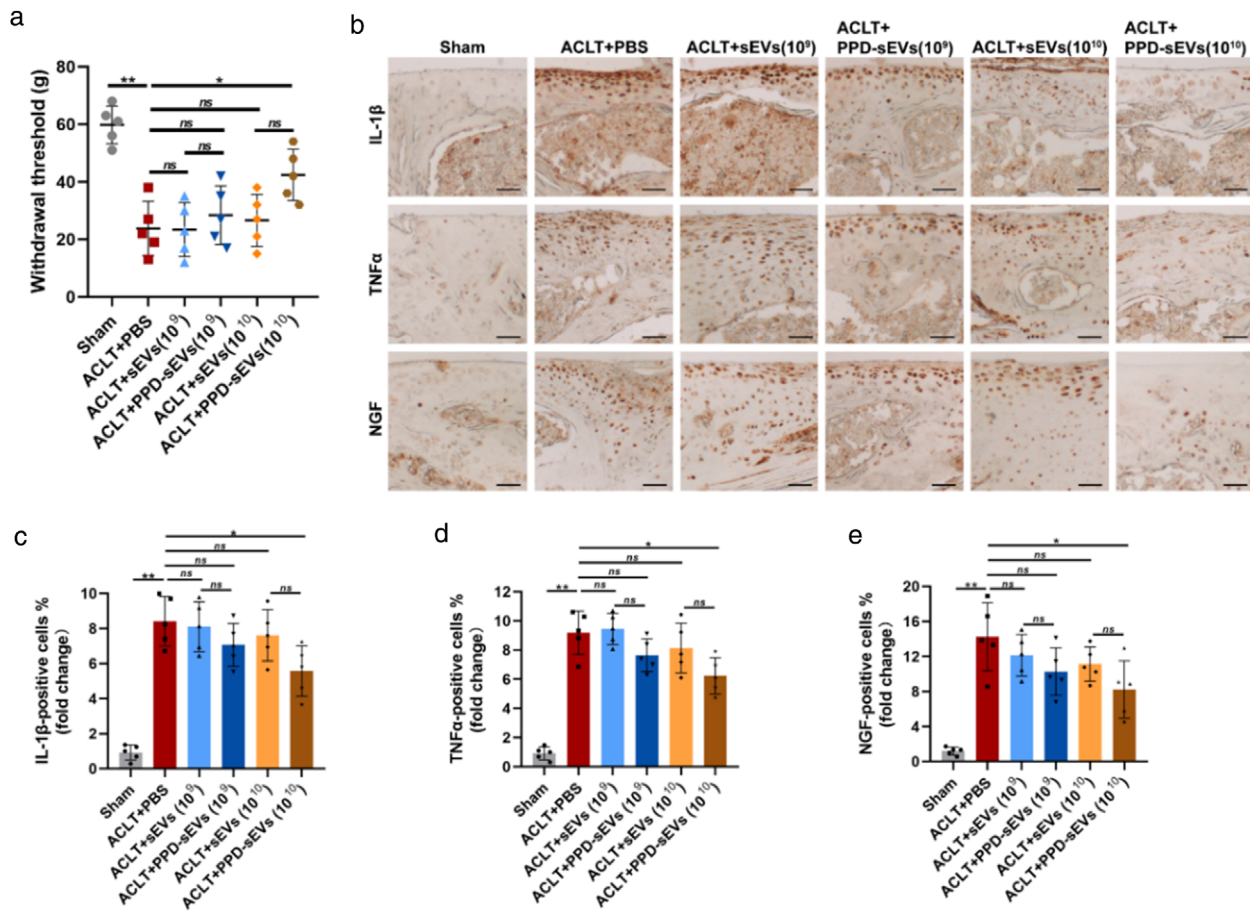
FIGURE 9 In vivo evaluation of PPD-sEVs for OA related pain in ACLT-induced mice. (A) Mechanical sensitivity was measured after ACLT surgery ($n = 5$). WT, withdrawal threshold; (B) Representative images of immunohistochemistry analysis for pain-related inflammatory cytokines including IL-1β, TNFα, and NGF in each group, scale bar: 100 μm; (C-E) Quantitative analysis of immunohistochemical staining of pain-related inflammatory markers ($n = 5$), the fold change of each marker in each group was normalized against the Sham group (vs. Sham group). *$P < 0.05$, **$P < 0.01$

clearance rate by lymphatics and sub-synovial capillaries N_{Exit} (Bajpayee & Grodzinsky, 2017). N_{Entry} should be fast enough to achieve a tendency of cartilage distribution rather than clearance from joint space. Unfortunately, the intrinsic physicochemical properties of cartilage matrix and local environment of joint cavity are very unfavourable to achieve a fast N_{Entry} of sEVs. Cartilage consists of dense (<6 nm mesh size) and negatively charged matrix, leading to a strong steric and electrostatic hinderance to sEVs which is displayed clearly in the cartilage uptake and penetration evaluation of this study with full thickness pig cartilage explant as a diffusive model (results in Figure 6B). Because of the hinderance, sEVs should mainly exist in synovial fluid after intra-articular injection. However, according to several previous reports, the administered nanoparticles are cleared very fast from joint space through lymphatics and sub-synovial capillaries (Edwards, 2011; Partain et al., 2020; Pradal et al., 2016). These factors result in low bioavailability of MSC-sEVs and give reason to why frequent injections of high dose MSC-sEVs are necessary in current studies (Cosenza et al., 2017; Zhang et al., 2016; Zhang et al., 2018; Zhang et al., 2019; Zhu et al., 2017). Furthermore, rodents with a thin layer of cartilage (~100 μm) are usually used in these studies to build OA model. However, human cartilage shows much larger thickness (~2.35 mm) than that of rodents, which may further increase the difficulty of sEVs biodistribution in cartilage and induce more compromised bioavailability (Ahern et al., 2009). Collectively, improving the distribution of MSC-sEVs in cartilage and thus increasing their bioavailability are critical for the future clinical application of MSC-sEVs in OA therapy.

Cationic nanocarriers have been widely studied and applied in intra-articular drug delivery (Brown et al., 2019; Colella et al., 2020; Vedadghavami et al., 2020). Up to now, several cationic nano-carriers such as avidin, polyamindoamine (PAMAM) dendrimer, cationic micelle, and artificial peptides have been successfully used to improve the biodistribution of loaded guest molecules in cartilage (Bajpayee et al., 2014; B. Geiger, Wang, Padera, Grodzinsky & Hammond, 2018; Vedadghavami et al., 2019; Wei et al., 2021). These carriers can adsorb to cartilage fast and show weak binding ability to anionic components in cartilage through electrostatic interaction. The fast adsorption can prevent their intra-articular clearance, while the weak binding to cartilage components can lead to their deep penetration and long-time retention in cartilage. Inspired by those cationic nanocarrier

strategy, for the first time, a surface charge reverse strategy of sEVs is successfully conducted to improve the biodistribution of sEVs in cartilage tissue.

The amphiphilic cationic polymer PPD is designed to reverse the surface charge of sEVs. PPD can bind sEVs by dual interaction, namely its electrostatic interaction with anionic surface and self-assembly to the bilayer lipid membrane of sEVs. Both interactions can be proved in the modification stability test of this study in which PPD shows more stable binding ability than that of εPL under HA or CS interference. PPD's resistance to anionic macromolecule interference is very critical to avoid its disassociation from sEVs membrane after intar-articular injection in consideration of the wide distribution of HA and CS in joint. In addition, as the spontaneous nature of electrostatic and self-assembly interaction, PPD modification can be achieved with a high efficacy by simple incubation in aqueous solution without the need of extra processes or agents in chemical lingation and artificial liposome fusion methods. PEI and cationic pullulan have been also used to modify sEVs by simple incubation via electrostatic binding. However, severe clusters of sEVs can be observed in those studies (Tamura et al., 2017; Zhupanyn et al., 2020). Furthermore, PEI can break the lipid membrane and shows severe biotoxicity, leading to their limited practical application in biology (Parhamifar et al., 2010). While, no cluster or morphology change of sEVs is observed after PPD modification. Besides, PPD also showed no impact on the contents of sEVs cargos and did not shield the function of sEVs surface proteins. We contribute this superior disturbance to the unique property of εPL. Unlike the widely used cationic polymers in building drug delivery carrier such as PEI, $α$-polylysine ($α$-PL), and PAMAM dendrimer, the exposed $α$-NH$_2$ groups in εPL present a lower protonation ability which means a relatively sparse positive charge density of εPL in physiological solution and minor disturbance to the structure and integrity of lipid membrane (Bankar & Singhal, 2013; K. Kim et al., 2018). And that is why εPL exhibits superior biocompatibility and can be widely used as a quite safe preservative in food industry (Tuersuntuoheti et al., 2019).

The surface charge of sEVs is reversed from negative to positive after PPD modification. Compared with the unmodified sEVs, the cartilage uptake, penetration, and joint retention capacity of the cationic PPD-sEVs is proved to be enhanced significantly. Furthermore, an increased chondrocyte uptake capacity is also demonstrated. The cellular internalization of extracellular vesicles is mainly carried out by endocytosis mechanism, and a positively charged surface may raise their contact probability with cell membrane (Costa Verdera et al., 2017). In addition, we notice a relatively slower cartilage uptake rate of PPD-sEVs than currently reported nanocarriers. For example, over 90% partially PEGlyted PAMAM dendrimer (G6, with IGF-1 conjugation) adsorb to cartilage explants in 24 h, while only 16 % ~ 33% PPD-sEVs adsorb to cartilage explants within the same duration (B. C. Geiger, Wang, Padera, Grodzinsky & Hammond, 2018). We think the slow uptake rate of PPD-sEVs should be caused by their large size, as those reported nanocarriers usually show size distribution smaller than 30 nm. The surface charge reverse strategy can break the electric hinderance effect of cartilage to sEVs, but it is unlikely to show impact on the cartilage steric hinderance. And it seems impossible to dramatically decrease the size distribution of sEVs to 30 nm given their cellular secretion mechanism.

Our previous studies have discovered the similar (or even better) therapeutic functions of sEVs from iMSC to (than) sEVs from adult MSC for many diseases treatment including OA (Liu et al., 2017; Zhu et al., 2017). While, compared with the adult MSC, iMSC are easily to be produced in large scale to generate sufficient sEVs for application and avoid the problem of cell source variation, resulting in the batch stability of the function and production of therapeutic sEVs. Thus, sEVs derived from iMSC were used in this study. Our previous study showed that weekly intra-articular injection of at least 1×10^{10} particles/ml of iMSC-sEVs (sEVs) is needful to induce a significant OA improvement in mouse model, and it is confirmed again in the present study where weekly injection of 10 $μ$l 1×10^9 particles/ml sEVs fails to improve the OA pathological features (Zhu et al., 2017). As a comparison, weekly injection of 10 $μ$l 1×10^9 particles/ml PPD-sEVs is sufficient to induce a significant improvement, demonstrating a much higher intra-articular bioavailability of PPD-sEVs than the unmodified sEVs. Considering the doubled half-life time of PPD-sEVs in joint to that of sEVs, we further reduced the injection frequency to once every two weeks, and 1×10^{10} particles/ml cationic PPD-sEVs can also alleviate the pathological features of OA. A higher bioavailability provides a possibility to reduce the dose and injection frequency, both of which are beneficial for the future clinical application of sEVs. However, due to the limitation of the mouse OA model, preclinical investigation is needed in larger animals in the future to further confirm the enhanced intra-articular bioavailability of PPD-sEVs. Moreover, lipophilic dyes including DiO, DiI, DiR were used in our study to label sEVs and these dyes could bind to the membrane fragments, causing the non-specific labelling. Therefore, a better sEVs labelling dye need to be developed in the future for avoiding the limitation.

In summary, we have established a surface charge reverse strategy to increase the intra-articular bioavailability of sEVs for OA improvement. By the facile incubation of sEVs with PPD in aqueous solution, a cationic surface of sEVs was accomplished and led to the generation of the PPD-sEVs. PPD modification showed negligible impact on the physiochemical properties of sEVs but increased their chondrocyte uptake capacity and further enhanced their chondrocyte homeostasis modulation ability. PPD-sEVs showed significantly enhanced cartilage uptake, cartilage penetration, and joint retention capacities in comparison with unmodified sEVs. Furthermore, in vivo study demonstrated an improved intra-articular bioavailability of PPD-sEVs for OA alleviation. All these results suggest the possibility of the surface charge reverse strategy of MSC-sEVs can be used to achieve a more efficient MSC-sEVs based OA therapy. And this strategy has great potential to be adopted in the future clinical application of MSC-sEVs for OA treatment.

CONFLICT OF INTEREST
The authors declare no conflict of interest.

AUTHOR CONTRIBUTIONS
Most of the experiments were performed by Kai Feng; Kai Feng and Yunlong Yang wrote the manuscript; Xuetao Xie and Haiyan Li designed part of the experiments and revised the manuscript; Ji Yuan and Liangzhi Gong performed part of the in vitro experiments; Zhaochen Zhu performed part of the in vivo experiments; Ji Yuan, Juntao Zhang, and Xuetao Xie provided technical and resource assistance throughout the project; Yunlong Yang and Yang Wang designed the experiments and provided funds.

REFERENCES
Ahern, B. J., Parvizi, J., Boston, R., & Schaer, T. P. (2009). Preclinical animal models in single site cartilage defect testing: A systematic review. *Osteoarthritis and Cartilage 17*, 705–713.

Arra, M., Swarnkar, G., Ke, K., Otero, J., Ying, J., Duan, X., Maruyama, T., Rai, M., O'Keefe, R., Mbalaviele, G., Shen, J., & Abu-Amer, Y. (2020). LDHA-mediated ROS generation in chondrocytes is a potential therapeutic target for osteoarthritis. *Nature Communications 11*, 3427.

Bajpayee, A. G., & Grodzinsky, A. J. (2017). Cartilage-targeting drug delivery: Can electrostatic interactions help? *Nature Reviews Rheumatology 13*, 183–193.

Bajpayee, A. G., Wong, C. R., Bawendi, M. G., Frank, E. H., & Grodzinsky, A. J. (2014). Avidin as a model for charge driven transport into cartilage and drug delivery for treating early stage post-traumatic osteoarthritis. *Biomaterials 35*, 538–549.

Bankar, S. B., & Singhal, R. S. (2013). Panorama of poly-ε-lysine. *RSC Advances 3*, 8586–8603.

Brown, S., Kumar, S., & Sharma, B. (2019). Intra-articular targeting of nanomaterials for the treatment of osteoarthritis. *Acta Biomaterialia 93*, 239–257.

Chen, B., Sun, Y., Zhang, J., Zhu, Q., Yang, Y., Niu, X., Deng, Z., Li, Q., & Wang, Y. (2019). Human embryonic stem cell-derived exosomes promote pressure ulcer healing in aged mice by rejuvenating senescent endothelial cells. *Stem Cell Research & Therapy 10*, 142.

Colella, F., Garcia, J. P., Sorbona, M., Lolli, A., Antunes, B., D'Atri, D., Barré, F. P. Y., Oieni, J., Vainieri, M. L., Zerrillo, L., Capar, S., Häckel, S., Cai, Y., & Creemers, L. B. (2020). Drug delivery in intervertebral disc degeneration and osteoarthritis: Selecting the optimal platform for the delivery of disease-modifying agents. *Journal of Controlled Release 328*, 985–999.

Cosenza, S., Ruiz, M., Toupet, K., Jorgensen, C., & Noel, D. (2017). Mesenchymal stem cells derived exosomes and microparticles protect cartilage and bone from degradation in osteoarthritis. *Scientific Reports 7*, 16214.

Costa Verdera, H., Gitz-Francois, J. J., Schiffelers, R. M., & Vader, P. (2017). Cellular uptake of extracellular vesicles is mediated by clathrin-independent endocytosis and macropinocytosis. *Journal of Controlled Release 266*, 100–108.

Danielsen, S., Strand, S., de Lange Davies, C., & Stokke, B. T. (2005). Glycosaminoglycan destabilization of DNA-chitosan polyplexes for gene delivery depends on chitosan chain length and GAG properties. *Biochimica Et Biophysica Acta 1721*, 44–54.

Edwards, S. H. R. (2011). Intra-articular drug delivery: The challenge to extend drug residence time within the joint. *The Veterinary Journal 190*, 15–21.

Eldridge, S., Nalesso, G., Ismail, H., Vicente-Greco, K., Kabouridis, P., Ramachandran, M., Niemeier, A., Herz, J., Pitzalis, C., Perretti, M., & Dell'Accio, F. (2016). Agrin mediates chondrocyte homeostasis and requires both LRP4 and alpha-dystroglycan to enhance cartilage formation in vitro and in vivo. *Annals of the Rheumatic Diseases 75*, 1228–1235.

Fischer, D., Bieber, T., Li, Y., Elsässer, H.-P., & Kissel, T. (1999). A novel non-viral vector for DNA delivery based on low molecular weight, branched polyethylenimine: Effect of molecular weight on transfection efficiency and cytotoxicity. *Pharmaceutical Research 16*, 1273–1279.

Geiger, B., Wang, S., Padera, R., Grodzinsky, A., & Hammond, P. J. S.t.m. (2018). Cartilage-penetrating nanocarriers improve delivery and efficacy of growth factor treatment of osteoarthritis. *Science Translational Medicine 10*.

Geiger, B. C., Wang, S., Padera Jr., F. P., Grodzinsky, A. J., & Hammond, P. T. (2018). Cartilage-penetrating nanocarriers improve delivery and efficacy of growth factor treatment of osteoarthritis. *Science Translational Medcine 10*, eaat8800

Glasson, S. S., Chambers, M. G., Van Den Berg, W. B., & Little, C. B. (2010). The OARSI histopathology initiative—Recommendations for histological assessments of osteoarthritis in the mouse. *Osteoarthritis and Cartilage 18 Suppl 3*, S17–23.

Gong, L., Chen, B., Zhang, J., Sun, Y., Yuan, J., Niu, X., Hu, G., Chen, Y., Xie, Z., Deng, Z. Li, Q., & Wang, Y. (2020). Human ESC-sEVs alleviate age-related bone loss by rejuvenating senescent bone marrow-derived mesenchymal stem cells. *Journal of Extracellular Vesicles 9*, 1800971.

Hu, G.-W., Li, Q., Niu, X., Hu, B., Liu, J., Zhou, S.-M., Guo, S.-C., Lang, H.-L., Zhang, C.-Q., Wang, Y., & Deng, Z. F. (2015). Exosomes secreted by human-induced pluripotent stem cell-derived mesenchymal stem cells attenuate limb ischemia by promoting angiogenesis in mice. *Stem Cell Research & Therapy 6*, 10.

Hu, H., Dong, L., Bu, Z., Shen, Y., Luo, J., Zhang, H., Zhao, S., Lv, F., & Liu, Z. (2020). miR-23a-3p-abundant small extracellular vesicles released from Gelma/nanoclay hydrogel for cartilage regeneration. *Journal of Extracellular Vesicles 9*, 1778883.

Huang, J., Zhao, L., Fan, Y., Liao, L., Ma, P. X., Xiao, G., & Chen, D. (2019). The microRNAs miR-204 and miR-211 maintain joint homeostasis and protect against osteoarthritis progression. *Nature Communications 10*, 2876.

Hunter, D. J., & Bierma-Zeinstra, S. (2019). Osteoarthritis. *The Lancet 393*, 1745–1759.

Hwang, D. W., Jo, M. J., Lee, J. H., Kang, H., Bao, K., Hu, S., Baek, Y., Moon, H. G., Lee, D. S., Kashiwagi, S. Henary, M., & Choi, H. S. (2019).Chemical modulation of bioengineered exosomes for tissue-specific biodistribution. *Advances in Therapy (Weinh) 2*.

Jeon, O. H., Kim, C., Laberge, R.-M., Demaria, M., Rathod, S., Vasserot, A. P., Chung, J. W., Kim, D. H., Poon, Y., David, N., Baker, D. J., van Deursen, J. M., Campisi, J., & Elisseeff, J. H. (2017). Local clearance of senescent cells attenuates the development of post-traumatic osteoarthritis and creates a pro-regenerative environment. *Nature Medicine 23*, 775–781.

Jhun, J., Cho, K. H., Lee, D. H., Kwon, J. Y., Woo, J. S., Kim, J., Na, H. S., Park, S. H., Kim, S. J., & Cho, M. L. (2021). Oral administration of Lactobacillus rhamnosus ameliorates the progression of osteoarthritis by inhibiting *Joint Pain and Inflammation. Cells 10*(5), 1057–1070.

Jiang, B., Yan, L., Wang, X., Li, E., Murphy, K., Vaccaro, K., Li, Y., & Xu, R. H. (2019). Concise review: Mesenchymal stem cells derived from human pluripotent cells, an unlimited and quality-controllable source for therapeutic applications. *Stem Cells 37*, 572–581.

Katz, J. N., Arant, K. R., & Loeser, R. F. (2021). Diagnosis and treatment of hip and knee osteoarthritis: A review. *Jama 325*, 568–578.

Kiani, C., Chen, L., Wu, Y., Yee, A. J., & Yang, B. B. (2002). Structure and function of aggrecan. *Cell Research 12*, 19–32.

Kim, J., Lee, H., Park, K., & Shin, S. (2020a). Rapid and efficient isolation of exosomes by clustering and scattering. *Journal of Clinical Medicine 9*(3), 650–664.

Kim, K., Ryu, K., Choi, Y. S., Cho, Y. Y., Lee, J. Y., Lee, H. S., & Chang Kang H. (2018). Effects of the physicochemical, colloidal, and biological characteristics of different polymer structures between alpha-poly(l-lysine) and epsilon-poly(l-lysine) on polymeric gene delivery. *Biomacromolecules 19*, 2483–2495.

Kim, K. H., Jo, J. H., Cho, H. J., Park, T. S., & Kim, T. M. (2020). Therapeutic potential of stem cell-derived extracellular vesicles in osteoarthritis: Preclinical study findings. *Laboratory Animal Research 36*, 10.

Lenzini, S., Bargi, R., Chung, G., & Shin, J. W. (2020). Matrix mechanics and water permeation regulate extracellular vesicle transport. *Nature Nanotechnology 15*, 217–223.

Li, T., Chubinskaya, S., Esposito, A., Jin, X., Tagliafierro, L., Loeser, R., Hakimiyan, A. A., Longobardi, L., Ozkan, H., & Spagnoli, A. (2019). TGF-β type 2 receptor–mediated modulation of the IL-36 family can be therapeutically targeted in osteoarthritis. *Science Translational Medicine 11*(491).

Liu, X., Yang, Y., Li, Y., Niu, X., Zhao, B., Wang, Y., Bao, C., Xie, Z., Lin, Q., & Zhu, L. (2017). Integration of stem cell-derived exosomes with in situ hydrogel glue as a promising tissue patch for articular cartilage regeneration. *Nanoscale 9*, 4430–4438.

Ma, P. L., Lavertu, M., Winnik, F. M., & Buschmann, M. D. (2017). Stability and binding affinity of DNA/chitosan complexes by polyanion competition. *Carbohydrate Polymers 176*, 167–176.

Mancuso, P., Raman, S., Glynn, A., Barry, F., & Murphy, J. M. (2019). Mesenchymal stem cell therapy for osteoarthritis: The critical role of the cell secretome. *Frontiers in Bioengineering and Biotechnology 7*, 9.

Mao, G., Zhang, Z., Hu, S., Zhang, Z., Chang, Z., Huang, Z., Liao, W., & Kang, Y. (2018). Exosomes derived from miR-92a-3p-overexpressing human mesenchymal stem cells enhance chondrogenesis and suppress cartilage degradation via targeting WNT5A. *Stem Cell Research & Therapy 9*, 247.

Mi, M., Shi, S., Li, T., Holz, J., Lee, Y. J., Sheu, T. J., Liao, Q., & Xiao, T. (2012). TIMP2 deficient mice develop accelerated osteoarthritis via promotion of angiogenesis upon destabilization of the medial meniscus. *Biochemical and Biophysical Research Communications 423*, 366–372.

Mow, V. C., Holmes, M. H., & Lai, W. M. (1984). Fluid transport and mechanical properties of articular cartilage: A review. *Journal of Biomechanics 17*, 377–394.

Parhamifar, L., Larsen, A. K., Hunter, A. C., Andresen, T. L., & Moghimi, S. M. (2010). Polycation cytotoxicity: A delicate matter for nucleic acid therapy—Focus on polyethylenimine. *Soft Matter 6*, 4001–4009.

Partain, B. D., Unni, M., Rinaldi, C., & Allen, K. D. (2020). The clearance and biodistribution of magnetic composite nanoparticles in healthy and osteoarthritic rat knees. *Journal of Controlled Release 321*, 259–271.

Piffoux, M., Silva, A. K. A., Wilhelm, C., Gazeau, F., & Tareste, D. (2018). Modification of Extracellular Vesicles by Fusion with Liposomes for the Design of Personalized Biogenic Drug Delivery Systems. *ACS nano 12*, 6830–6842.

Pradal, J., Maudens, P., Gabay, C., Seemayer, C. A., Jordan, O., & Allemann, E. (2016). Effect of particle size on the biodistribution of nano- and microparticles following intra-articular injection in mice. *International Journal of Pharmaceutics 498*, 119–129.

Ruiz, M., Toupet, K., Maumus, M., Rozier, P., Jorgensen, C., & Noel, D. (2020). TGFBI secreted by mesenchymal stromal cells ameliorates osteoarthritis and is detected in extracellular vesicles. *Biomaterials 226*, 119544.

Sato, Y. T., Umezaki, K., Sawada, S., Mukai, S. A., Sasaki, Y., Harada, N., Shiku, H., & Akiyoshi, K. (2016). Engineering hybrid exosomes by membrane fusion with liposomes. *Scientific Reports 6*, 21933.

Shima, S., & Sakai, H. (1977). Polylysine produced by Streptomyces. *Agricultural Biological Chemistry 41*, 1807–1809.

Stell, G., & Joslin, C. G. (1986). The donna equilibrium: A theoretical study of the effects of interionic forces. *Biophisical Journal 50*, 855–859.

Tamura, R., Uemoto, S., & Tabata, Y. (2017). Augmented liver targeting of exosomes by surface modification with cationized pullulan. *Acta Biomaterialia*.

Tofiño-Vian, M., Guillén, M., Pérez Del Caz, M., Castejón, M., Alcaraz, M. J. O.m., & longevity, c. (2017). Extracellular vesicles from adipose-derived mesenchymal stem cells downregulate senescence features in osteoarthritic osteoblasts. *Oxidative Medicine and Cellular Longevity 2017*, 7197598.

Tuersuntuoheti, T., Wang, Z., Wang, Z., Liang, S., Li, X., & Zhang, M. (2019). Review of the application of ε-poly-L-lysine in improving food quality and preservation. *Journal of Food Processing and Preservation 43*, e14153.

Vedadghavami, A., Wagner, E. K., Mehta, S., He, T., Zhang, C., & Bajpayee, A. G. (2019). Cartilage penetrating cationic peptide carriers for applications in drug delivery to avascular negatively charged tissues. *Acta Biomaterialia 93*, 258–269.

Vedadghavami, A., Zhang, C., & Bajpayee, A. G. (2020). Overcoming negatively charged tissue barriers: Drug delivery using cationic peptides and proteins. *Nano Today 34*.

Wang, C., Luo, X., Zhao, Y., Han, L., Zeng, X., Feng, M., Pan, S., Peng, H., & Wu, C. (2012). Influence of the polyanion on the physico-chemical properties and biological activities of polyanion/DNA/polycation ternary polyplexes. *Acta Biomaterialia 8*, 3014–3026.

Wehling, P., Evans, C., Wehling, J., & Maixner, W. (2017). Effectiveness of intra-articular therapies in osteoarthritis: A literature review. *Therapeutic Advances in Musculoskeletal Disease 9*, 183–196.

Wei, Y., Luo, L., Gui, T., Yu, F., Yan, L., Yao, L., Zhong, L., Yu, W., Han, B., Patel, J. M., Liu, J. F., Beier, F., Levin, L. S., Nelson, C., Shao, Z., Han, L., Mauck, R. L., Tsourkas, A., Ahn, J., … Qin, L. (2021). Targeting cartilage EGFR pathway for osteoarthritis treatment. *Science Translational Medcine 13*, eabb3946.

Witwer, K. W., Van Balkom, B. W. M., Bruno, S., Choo, A., Dominici, M., Gimona, M., Hill, A. F., De Kleijn, D., Koh, M., Lai, R. C., Mitsialis, S. A., Ortiz, L. A., Rohde, E., Asada, T., Toh, W. S., Weiss, D. J., Zheng, L., Giebel, B., Lim, S. K. (2019).Defining mesenchymal stromal cell (MSC)-derived small extracellular vesicles for therapeutic applications. *Journal of Extracellular Vesicles 8*, 1609206.

Woo, C. H., Kim, H. K., Jung, G. Y., Jung, Y. J., Lee, K. S., Yun, Y. E., Han, J., Lee, J., Kim, W. S., & Choi, J. S., Yang, S., Park, J. H., Jo, D-G., Cho, Y. W. (2020).Small extracellular vesicles from human adipose-derived stem cells attenuate cartilage degeneration. *Journal of Extracellular Vesicles 9*, 1735249.

Wu, J., Kuang, L., Chen, C., Yang, J., Zeng, W. N., Li, T., Chen, H., Huang, S., Fu, Z., Li, J., Liu, R., Ni, Z., Chen, L., Yang, L. (2019).miR-100–5p-abundant exosomes derived from infrapatellar fat pad MSCs protect articular cartilage and ameliorate gait abnormalities via inhibition of mTOR in osteoarthritis. *Biomaterials 206*, 87–100.

Xia, Y., Hu, G., Chen, Y., Yuan, J., Zhang, J., Wang, S., Li, Q., Wang, Y., & Deng, Z. (2021). Embryonic stem cell derived small extracellular vesicles modulate regulatory T cells to protect against ischemic stroke. *ACS Nano 15*, 7370–7385.

Yang, Y., Zhu, Z., Gao, R., Yuan, J., Zhang, J., Li, H., Xie, Z., & Wang, Y. (2021). Controlled release of MSC-derived small extracellular vesicles by an injectable Diels-Alder crosslinked hyaluronic acid/PEG hydrogel for osteoarthritis improvement. *Acta Biomaterialia. 128*, 163–174. https://doi.org/10.1016/j.actbio.2021.1004.1003

Zhang, S., Chu, W. C., Lai, R. C., Lim, S. K., Hui, J. H., & Toh, W. S. (2016). Exosomes derived from human embryonic mesenchymal stem cells promote osteochondral regeneration. *Osteoarthritis and Cartilage 24*, 2135–2140.

Zhang, S., Chuah, S. J., Lai, R. C., Hui, J. H. P., Lim, S. K., & Toh, W. S. (2018). MSC exosomes mediate cartilage repair by enhancing proliferation, attenuating apoptosis and modulating immune reactivity. *Biomaterials 156*, 16–27.

Zhang, S., Teo, K. Y. W., Chuah, S. J., Lai, R. C., Lim, S. K., & Toh, W. S. (2019). MSC exosomes alleviate temporomandibular joint osteoarthritis by attenuating inflammation and restoring matrix homeostasis. *Biomaterials 200*, 35–47.

Zhu, Y., Wang, Y., Zhao, B., Niu, X., Hu, B., Li, Q., Zhang, J., Ding, J., Chen, Y., & Wang, Y. (2017). Comparison of exosomes secreted by induced pluripotent stem cell-derived mesenchymal stem cells and synovial membrane-derived mesenchymal stem cells for the treatment of osteoarthritis. *Stem Cell Research & Therapy 8*(1), 64–74.

Zhupanyn, P., Ewe, A., Buch, T., Malek, A., Rademacher, P., Muller, C., Reinert, A., Jaimes, Y., & Aigner, A. (2020). Extracellular vesicle (ECV)-modified polyethylenimine (PEI) complexes for enhanced siRNA delivery in vitro and in vivo. *Journal of Controlled Release 319*, 63–76.

SUPPORTING INFORMATION

Additional supporting information may be found in the online version of the article at the publisher's website.